Republic of Iraq

Ministry of Higher Education

And Scientific Research

University of Babylon

College of Materials Engineering

Department of Metallurgical Engineering

Modification of the Microstructure and Mechanical Properties of Gas Metal Arc Additive Manufacturing Mild Steel by the Forging Process

A Dissertation

Submitted to the Council of the College of Materials Engineering/ University of Babylon in Partial Fulfillment of The Requirements for the Master Degree in Materials Engineering/Metallurgical

By

Arzaq Saleem Abd Ali Al-roubaiy

Supervised by

Prof. Saad Hameed Al-Shafaie (Ph.D.)

Asst. Prof. Abdul Sameea Jasim Abdul Zehra Jilabi (Ph.D.)

2023 A.D **1445 A.H**

بسم الله الرحمن الرحيم

(قَالُواْ سُبۡحَٰنَكَ لَا عِلۡمَ لَنَآ إِلَّا مَا عَلَّمۡتَنَآۖ
إِنَّكَ أَنتَ ٱلۡعَلِيمُ ٱلۡحَكِيمُ) (32)

صدق الله العلي العظيم

(سورة البقرة اية 32)

Supervisor Certificate

I certify that this dissertation entitled **(Modification of the Microstructure and Mechanical Properties of Gas Metal Arc Additive Manufacturing Mild Steel by the Forging Process**) is prepared by **(Arzaq Saleem Abd Ali Al-roubaiy)** under my supervision at the Department of Metallurgical Engineering/ Faculty of Materials Engineering/University of Babylon in partial fulfillment of the requirements for the Master Degree in Material's Engineering/Metallurgical Engineering.

Name of Supervisor:

Prof. Saad Hameed Al-Shafaie

Date: / /2021

Name of Supervisor:

Assist. Prof. Dr. Abdul Sameea J. A. Z. Jilabi

Date: / /2023

Examining Committee Approval sheet

We certify that have read this dissertation entitled **(Modification of the Microstructure and Mechanical Properties of Gas Metal Arc Additive Manufacturing Mild Steel by the Forging Process)** and as an examining committee, we have examined the student **(Arzaq Saleem Abd Ali Al-roubaiy)** in contents and that is related to it, and that in our opinion it meets the standard of a dissertation for the Master degree in Materials Engineering/Metallurgical Engineering.

Prof. Dr. Jasim Mohammed Salman

Committee Chair

Date: / /2023

Dr.Ahmad Ameed Zainalabdeen

Committee Member

Date : / / 2023

Asst. Porf. Dr. Basem Mohysen

Committee Member

Date : / / 2023

Prof. Saad Hameed Al-Shafaie

Supervisor

Date : / / 2023

Asst. Prof.Dr. Abdul Sameea Jasim Abdul Zehra Jilabi

Supervisor

Date : / / 2023

Approval of the Department
of Metallurgical Engineering

Head of Metallurgical Engineering Department

Prof. Dr. Haydar H.J. Jamal Al Deen

Date : / / 2023

Approval of the Department
of Metallurgical Engineering

Dean of The Faculty of Materials Engineering

Prof. Dr. Abdul Raheem K. Abid Ali

Date : / / 2023

Dedication

To the one who taught me to be proud

Respected father

To the source of giving and generosity

Revered mother

For someone who is closer to my soul

My loving husband

To my pulse and the secret of my joy

My dear daughter

To all those I received advice, support and assistance

I present to you the epitome of effort and exhaustion

§ § § § § §

Acknowledgements

Foremost, praise be to ALLAH for the blessings of age, mind and health He bestowed upon me and the determination and patience with which I challenged the difficulties I encountered during the completion of this research.

My sincere appreciation and deepest gratitude are due to the Department of Metallurgical Engineering, I would like to thank **Prof.Dr. Saad Hameed Al-Shafaie** and **Asst. Prof.Dr. Abdul Sameea Jasim Abdul Zehra Jilabi** whom I had the honour of being under their guidance and supervision, their constructive suggestion, patience and continuous encouragement are highly acknowledged through this study.

Finally, I extend my thanks and appreciation to my family, my parents, and my husband and all the friends for their financial and moral support throughout the study period and my beloved daughter, Narjis who was my inspiration pursue this quest.

ABSTRACT

Recently, Metal Inert Gas (MIG)-based weld deposition process is one of the deposition-based Additive Manufacturing (AM) processes. This technique has created considerable interest due to the advantages it offers of being able to produce fully functional, complex, dense metallic objects. Because of the high deposition rates, high material and power efficiency, lower investment costs, simpler setup and work environment requirements, it is becoming a viable metallic AM method.Nowadays, AM technologies are used in a wide range of applications such as automotive manufacturers, machine tool industry and aerospace companies …etc.

The study mainly aims to investigate the influence of a variety of deposition patterns and the cold forging process with different hammer strokes (5) HS and (3) HS on the microstructure and the mechanical properties of steel materials built on a low alloy steel substrate by MIG process. Experiments were carried out using a semi-automated MIG welding on AISI 5155 low alloy steel substrate using (ER70S.6) copper coated steel wire to built the samples manufactured using five different deposition patterns (longitudinal, transverse, right network, oblique and oblique network). Several examinations were performed to evaluate the samples built with and without the forging process using optical microscopy, scanning electron microscopy with energy dispersive spectrometry and fractography, in addition to mechanical tests such as microhardness and the tensile strength.

The results revealed that the samples built by the different deposition patterns showed a diversity of microstructure in different regions. Microscopy generally showed coarse equiaxed grains in the lower regions، fine equiaxed grains in the middle regions and columnar grains in the upper regions. The effect of the forging process on samples built with the different deposition patterns was

limited to the upper regions of the deposited material where the resulting microstructures were elongated grains. The hardness of the samples forged by (5) HS was higher than that of those forged by (3) HS. The maximum hardness was (258 HV) for the sample built with the oblique network pattern and forged by (5) HS, while the minimum hardness was (170 HV) for the sample built longitudinally without forging. Cold forging introduced, in general, a noticeable increase in tensile strength of the specimens extracted from the different samples. The highest average tensile strength value was (562MPa) for the sample built longitudinally and forged by (3) HS. The fracture mode was significantly ductile. The lowest average tensile strength value was however (263MPa) for the sample built transversely, and the fracture mode was brittle.

List of Tables

List of Figures

List of Abbreviations

Abbreviation	Express
AC	Alternating Current
AM	Additive Manufacturing
ASRC	Alloy Steel Research Commission
ASTM	American Society for Testing Materials
AWS	American Welding Society
BM	Base Metal
BTF	Buy-To-Fly ratio
CAD	Computer-Aided Design
CE	Carbon Equivalent
CGHAZ	Coarse Grained Heat Affected zone
DC	Direct Current
DMLS	Direct Metal Laser Sintering
DED	Directed Energy Deposition
DCSP	Direct Current Straight Polarity
DCEN	Direct Current Electrode Negative
DCRP	Direct Current Reverse Polarity
DCEP	Direct Current Electrode Positive
DLF	Direct Laser Fabrication
FGHAZ	Fine Grained Heat Affected zone
GMAW	Gas Metal Arc Welding

GTAW	Gas Tungsten Arc Welding
HAZ	Heat Affected Zone
ICHAZ	Intercritical Heat Affected zone
LMD	Laser Metal Deposition
MIG	Metal Inert Gas
PAW	Plasma Arc Welding
PBF	Powder Bed Fusion
RP	Rapid Prototyping
SLM	Selective Laser Melting
SM	Shape Melting
SW	Shape Welding
SMD	Shape Metal Deposition
SFF	Solid Freeform Fabrication
SMAW	Shielded Metal Arc Welding
SCHAZ	Subcritical Heat Affected zone
WAAM	Wire Arc Additive Manufacturing

List of Content

CHAPTER ONE:

INTRODUCTION

INTRODUCTION

1.1 General View

In the new manufacturing technique known as additive manufacturing (AM), a component is created using layer by layer deposition of the raw material to create a dense, completely operational and three-dimensionally formed component **[1,2]**. AM, provides a number of possible advantages. The ability to produce complicated geometries with more design freedom than traditional manufacturing and a shorter supply chain due to the ability to print parts as needed rather than keeping them in stock are two of these advantages. **[3]**. Using diverse AM processes, a large variety of different metals, ceramics, composites, and polymers can be employed as the raw material. The three main categories of powder bed processes, such as selective laser melting (SLM) or direct metal laser sintering (DMLS), powder-feed processes, such as laser metal deposition (LMD),are also known as direct laser fabrication (DLF), and directed energy deposition techniques (DED). In which focused thermal energy is used to melt the feedstock materials, can be used to categorize the additive manufacturing of metallic components. **[4, 5]**.

One of the DED technology types is of wire arc additive manufacturing (WAAM), an additive manufacturing technique that typically uses a robotic arm and an arc welding flame to create metallic items by layering weld beads on top of previously deposited layers. **[6, 7]**. Because WAAM has the potential to generate massive metallic components with moderate geometric complexity, it is suggested as a promising alternative to conventional subtractive techniques. Due to the benefits it offers, such as low cost and high deposition rates in compared to other additive manufacturing

techniques, this technology has recently generated interest. Depending on the nature of the heat source, there are three types of WAAM:

- GMAW/MIG (Gas Metal Arc Welding).
- GTAW/TIG (Gas Tungsten Arc Welding).
- PAW (Plasma Arc Welding).

The most significant benefit of the WAAM method, given its nature and the need for economic competitiveness, is the high deposition rate achieved in comparison to other additive manufacturing technologies. Generally, based on the properties of the material and process parameters, deposition rates of the GMAW range from 1 to 10 kg/h **[8]**, which, based on GTAW and PAW, is between two and three times greater than those achieved using WAAM methods. Nonetheless, AM techniques are currently being heavily used in a number of sectors, including automotive manufacturers, machine tool industry, aerospace companies, medicinal industries, construction and architectural industries [**9]**. Due to the wide variety of mechanical and chemical qualities, several materials can be used in additive manufacturing. The range of materials used in 3D printing is constantly expanding, as seen by the industrial applications of this technology. In the coming years, it has expected that the demand for 3D printing systems, materials software, and related products would be increased by 22.3% annually **[10]**. Moreover, ID Tech Ex predicts that by 2029, $23 billion would be invested in 3D printing materials globally**[11].**

1.2 The Aims of this Work

1. Study the effect of using a variety of deposition patterns on the mechanical properties and the microstructure of (ER70S.6) mild steel material built on an AISI5155 low alloy steel substrate by the WAAM.
2. Study the effect of cold forging on the microstructure and as a result the mechanical properties of these materials deposited by different patterns.

1.3 Dissertation Outline

This chapter deals with a general introduction in addition to the objectives of this study. Chapter two includes the theoretical part of this dissertation. In this part, AM will be described starting from definition, advantages and disadvantages, types and applications. This chapter deals with the literature review related to the current work. The third chapter provides a description of the experimental part in terms of using low alloy steel as substrate material, and the low carbon steel wire with copper coating (ER70S-6) as an additive metal, in addition to the deposition technology and the forging process. The built-up and preparation of the specimens for mechanical and physical testing are also described.

In chapter four, the results of the experimental work on low alloy steel substrates by AM technology are analyzed and discussed. Chapter five consists of the conclusions and suggestions for future works.

CHAPTER TWO:

THEORETICAL PART &

LITERATURE REVIEW

THEORETICAL PART AND LITERATURE REVIEW

2.1 Introduction

This chapter deals with low alloy steels and their weldability, and provides general information about additive manufacturing processes and their classification. It also emphasis on wire arc additive manufacturing (WAAM), especially the MIG method, the method used in this study, its advantages, limitations and most important applications. This chapter also explains the effect of the forging process on additive manufactured products before presenting a literature review on the dissertation topic.

2.2 Low Alloy Steels

The Alloy Steel Research Commission (ASRC) defines carbon steel as steel with a manganese content of no more than 0.5% and silicon of no more than 0.5%, while for other types of steel they are considered alloy steels **[12]**. Alloy steels have been developed to overcome the limitations caused by the use of carbon steels in order to meet the demands of the engineering organization, where **[13,14]**:

1. It is difficult to obtain a tensile strength greater than 700 N/mm^2 while maintaining proper ductility and toughness.
2. There is an exposure to cracking risks while severe quenching by water necessary to achieve full hardening.
3. Plain carbon steels are susceptible to “mass effect” which makes it difficult to harden large sections effectively.
4. Plain carbon steels are prone to corrosion and oxidation.

Alloy steels can be categorized to three kinds: low, medium and high alloy steels **[15]**. Low alloy steels can be classified based on **[16]**:

1. The chemical composition of steels based on the primary additives such as Ni steels, Mo steels, Ni–Cr steels, Cr–Mo steels and so on.
2. Heat treatments like annealed steels, normalized and tempered steels, quenched and tempered steels and so on.
3. The weldability.

Low alloy steels are typically used in bridges, power transmission towers, industrial equipment, light poles, oil and gas pipelines, storage tanks, off-road and heavy-duty high-way vehicles. Passenger car components, farm and construction machinery, building beams and panels, mine and railroad cars, and lawn mowers among other applications **[17,18]**.

2.2.1 Alloying Elements

The following are the most common alloying elements added to steels **[19]**:

1. Carbon: influences machinability, tensile strength, hardness and the melting point.
2. Manganese: contributes to the hardness and strength of steel. When present in relatively high weight percentages with high carbon content in steel, it reduces ductility and weldability.
3. Silicon: boosts the strength of low alloy steels and improves resistance to oxidation.
4. Nickel: rises toughness and impact resistance. A high percentage of it enhances corrosion resistance.
5. Chromium: is added to increase deep hardenability and abrasion resistance. It also aids in the prevention of corrosion and oxidation.
6. Molybdenum: increases steel hardenability, small grain size, and creep and tensile strength at high temperatures. In Ni-Cr steels, it also helps to reduce temper brittleness.

7. Vanadium: enhances fine grains in steels while maintaining ductility and increasing strength.
8. Tungsten: when added to steels, it increases hardness and strength at high temperatures, resists heat, and improves fine grain appearance.
9. Cobalt: participates in the hardening of ferrite to achieve red-hardness.
10. Copper: when added to steels at a concentration of 0.2-0.5 percent, it improves atmospheric corrosion resistance and acts as a strengthening element.
11. Aluminum: it produces fine austenitic grains and acts as a deoxidizer.
12. Sulphur: increases machinability while also lowering ductility and weldability.
13. Boron: (0.001-0.003%) is a strong hardening agent.

2.3 Principle of Additive Manufacturing

On a fixtureless platform, AM involves the creation of a product in the form of pre-defined slices of layers. The products generated by AM technologies follow an "Additive" principle, in contrast to traditional subtractive manufacturing methods, in which the process begins with a block of material and undesired material is gradually removed until the desired item is obtained. "Progressive addition of small slices of feedstock layers in a layer-upon-layer fashion" is how AM is characterized. This indicates that the raw feedstock material has been selectively deposited in a pre-determined format, and the process is referred to as "Additive Manufacturing" as a whole. Physical components are manufactured from virtual computer-aided models in AM systems. Furthermore, AM begins with a blank canvas and creates a part layer by layer, depositing each new layer on top of the preceding one until the part is complete. Depending on the material and the AM method used, the layer thickness can range from a few microns to about 0.25 mm **[20]**. When compared to traditional

subtractive manufacturing, AM's unique principle and manufacturing capability offer the following benefits **[21]**: AM allows a computer-aided design (CAD) to be instantly translated into a finished/semi-finished product without the need for extra fixtures or cutting tools. Furthermore, the AM principle allows for the creation of complicated and detailed objects that would otherwise be impossible to create using traditional machining methods. Hard-to-machine metals and alloys can also be fabricated using advanced AM techniques. In summary, the AM principle promotes environmental friendliness, design flexibility and lean functional component manufacture. Some AM processes, like as fused deposition modeling, however, utilize a support material to aid the manufacture of overhanging areas of goods. The construction of such support structures has similarly followed the "Additive" principle; however, the materials employed have varied **[20,21]**.

2.4 Classification of Additive Manufacturing Technologies

AM processes come in a wide range of types. For novices to the profession, the vast array of options can be bewildering. Furthermore, to set themselves apart from their competitors, AM system manufacturers have coined distinct process names, adding to the confusion. The ASTM International Committee on Additive Manufacturing Technologies approved a collection of AM process category terminology and definitions in January 2012 **[22]**. Below is a list of ASTM-approved AM process words, along with a standardized definition **[23]**.

1. Binder Jetting: A liquid bonding agent is selectively placed to combine powder materials.

2. Directed Energy Deposition: in which concentrated heat energy is employed to melt materials as they are deposited, fusing them together.

3. Material extrusion: in which material is distributed selectively through a nozzle or aperture.

4. Material Jetting: in which build material droplets are placed selectively.

5. Powder Bed Fusion: in which thermal energy is used to selectively fuse powder bed regions.

6. Sheet Lamination: in which material sheets are glued together to make an object.

7. Vat Photo Polymerization: A light-activated polymerization skill used to selectively cure liquid photopolymer in a vat.

The AM system that is most significant in this dissertation is Direct Energy Deposition (DED). Since DED is regarded as the most convenient manufacturing process for prototyping and direct part production, it will be the subject of this dissertation.

2.5 Directed Energy Deposition

Directed energy deposition (DED) is a type that can treat a wide range of materials, including polymers, ceramics and metal alloys. The method is most typically utilized for metal powder, and is referred to as "Metal Deposition Technology" on occasion **[24]**. All approaches in which a wire or powder feedstock is directly deposited into a melt pool formed by focused energy fall into this category. Unlike powder bed fusion (PBF), the material is melted as it is deposited, rather than being pre-laid into a powder bed. The origins of this AM method can be traced back to a welding procedure in which a wire is melted by an arc **[25]**. Figure (2.1) shows a schematic illustration of a typical DED system **[26]**. The melt pool is created by focused energy, which can be a laser beam, an electron beam or a plasma arc. The most widely used commercialized technology however combines a laser with a powder deposition device.

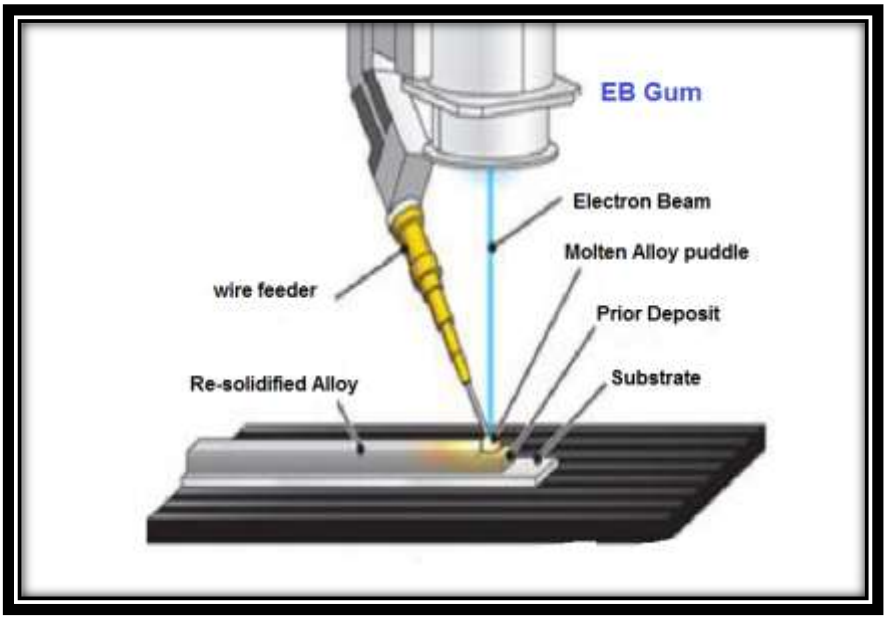

Figure (2.1): Schematic illustration of a wire-fed DED process **[26].**

2.6 Benefits and Limitations with Directed Energy Deposition

Because there is no requirement for a pre-laid powder bed, DED allows for a bigger build volume. The size of the gas/vacuum filled chamber or the operating envelope of the deposition head are the key design constraints for these machines. The machines in which the shield gas is delivered out of the deposition head fall into another category. Additional distinct advantage of DED procedures is their ability to be integrated with existing subtractive technologies, as well as their utility in the field of repairs. Because the machine only has the last laid layer as support for creating the next layer of material, DED procedures necessitate support structures and/or unique arrangements to create complex geometries such as cavities or undercuts. DED, like many other AM processes, frequently necessitates post-processing such as substrate/support structure removal and/or thermal treatment to relieve tensions. However, DED's biggest Limitations is its poor surface polish, which means that the parts usually require additional machining to satisfy their specifications **[24]**.

2.7 Wire Arc Additive Manufacturing Process

The process of depositing weld metal to produce whole components has been employed since 1920, and it is today known as wire arc additive manufacturing (WAAM). This approach offers various advantages over traditional production methods, including a higher buy-to-fly (BTF) ratio, the flexibility to possibly ignore the size limit of component fabrication, and cost-effectiveness as compared to powder-based procedures that rely on expensive materials **[27]**. According to ASTM F2792-12a, WAAM is a wire-feed AM method that includes indirect energy deposition (DED) **[28]**. It is also known as an electric arc heat source and a raw material formed of metal wire. The concept of WAAM is based on the automatic welding process. WAAM has been referred to as rapid prototyping (RP), shape melting (SM) and shape welding (SW), shape metal deposition (SMD), solid freeform fabrication (SFF), and even 3D welding in recent years **[29]**.

2.7.1 Classification of Wire Arc Additive Manufacturing

Depending on the nature of the heat source, there are three types of WAAM approaches (Figure 2.2) **[28]**: GMAW (Gas Metal Arc Welding), GTAW (Gas Tungsten Arc Welding) and PAW (Plasma Arc Welding).

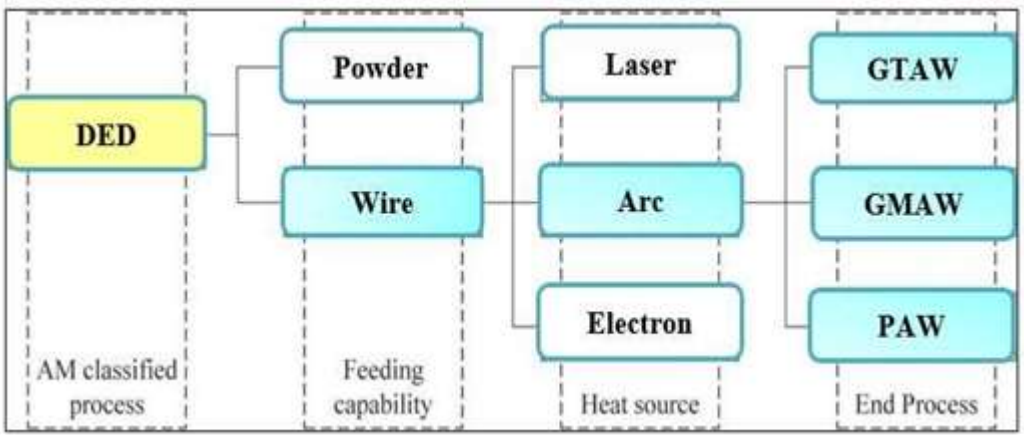

Figure (2.2): Typical classification of WAAM **[27].**

A consumable wire electrode and the workpiece metal generate an electric arc in the GMAW process, where the wire is typically perpendicular to the

substrate. Because of its high deposition rate and low heat input, a modified GMAW variation based on a controlled dip transfer mode mechanism has been widely adopted for AM procedures **[30,31]**. The weld in GTAW and PAW is made with a non-consumable tungsten electrode. In contrast to GMAW, the wire feed angle in GTAW and PAW is changeable and influences the deposit quality, making process planning more difficult **[29].** GMAW-based WAAM has a 2-3 times higher deposition rate than GTAW- or PAW-based techniques. The processing conditions and production rate for a target component are directly influenced by the WAAM technology **[32]**.

2.8 Gas Metal Arc Welding

It is an electric arc welding process in which fusion occurs as a result of heating the workpiece with the heat of the electric arc arising between it and the continuous feeding metal wire. No flux is used with this process, where the arc and the molten metal are covered with an inert gas, which may be argon or helium or with a gaseous covering may be carbon dioxide or a gaseous mixture **[33]**. Figure (2.3) presents a schematic of this process.

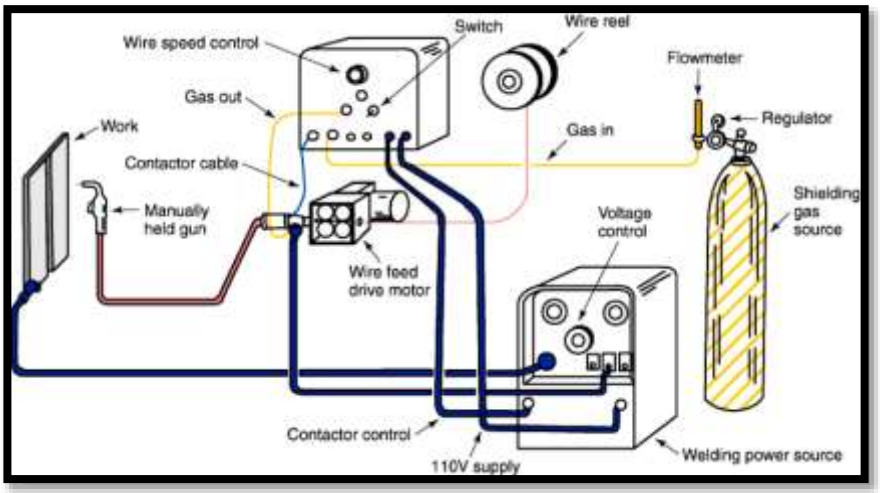

Figure (2.3): Schematic of gas metal arc welding process [34].

2.8.1 Working Principle

Before the arc igniting process can begin, the flow of gas and water must be assured. The suitable welding current and wire feeding speed, as well as the electrical connecting points, must be adjusted. As is customary when employing the arc, the arc is started by firing the electrode with the workpiece. Before the arc is ignited, about 15 mm of welding wire juts from the torch tip **[35]**. During welding, the torch should be kept at a distance of 10-12 mm from the workpiece with an arc length of 1.5-4 mm. To perform welding, the torch is moved along the weld joint steadily. The angle of the torch is within 70° with the horizon. The arc length is kept constant during welding using the principle of self-adjusting arc and self-controlled arc. The first is used in the case of semi-automatic welding (manual welding works), while the second is used with the automatic welding. Here is a brief idea of them **[36]**:

1. **Self-adjusting arc**: In the case of semi-automatic welding, the welding wire is fed from a spool through grooved rollers that rotate by a constant speed motor. Assuming that under certain conditions the arc length decreases, a decrease in voltage and an increase in welding current results. The increased welding current will cause the welding wire to melt at a faster rate, thus increasing the arc length to the required normal length. The opposite will happen if the arc length is longer than the required value.
2. **Self-controlled arc**: In the case of automatic welding, the welding wire is fed from a spool through grooved rollers rotated by an electric motor at variable speeds according to the change in the arc voltage. The speed increases when the voltage increases and vice versa. Under certain conditions, when the arc length increases, the arc voltage will increase, so the electric motor speed and wire feed rate will increase. Thus obtaining the desired natural arc length **[37]**.

2.8.2 Welding Equipment

Power sources used with GMAW (Metal Inert Gas (MIG) is another common name) are either direct current (DC) generators or alternating current (AC) transformers with rectifiers. It is generally not recommended to use the AC. As for the welding torch, which feeds the welding wire and covering gases, it may be of air-cooled or water-cooled type. Generally, a torch operating at amperage values above 200A is water cooled; the torch may have a straight or curved nozzle. The curved nozzle torch is usually used for welding complex components. The wire feeding mechanism supplies the wire from the spool to the welding torch at a constant or variable speed. The wire spool can be placed separately when using semi-automatic welding machines in order to facilitate welding over a wider area, while this feature is not present in automatic welding machines. There are welding wires of different diameters (0.8, 1, 1.2, 1.6 mm etc.). Standard wire spools may contain (1-15 kg) of wire. Steel wires are generally coated with copper. The chemical composition of the workpiece and wire should be as similar as possible; there are wires available for welding aluminum, magnesium, nickel and their alloys, as well as for welding low-alloy steel and stainless steel etc. The purpose of the covering gases is to protect the molten metal and the wire end from atmospheric pollutants **[38]**.

2.8.3 Polarity

When welding using DC, the welding arc is relatively smooth and stable because the DC flows in one direction during the welding cycle. The AC, however, collects the straight and reverse polarity (direction of the current flow) alternatively in regular cycles. These cycles are repeated periodically during welding, as the polarity frequents 100 times per second in 50 cycles. These frequencies result in an extremely fast pulsating arc, causing somewhat roughness and less stability compared to the DC arc.

Polarity is a significant factor when welding with DC. Choosing the kind of polarity depends on several significant factors such as the type of metal being welded and the type of penetration desired **[39]**.

1. Straight Polarity:

The DC used with this polarity is usually called direct current straight polarity (DCSP). With straight polarity, the current flows from the workpiece, which is connected with the positive terminal of the power supply to the wire, which is negatively charged. Therefore, this polarity is also called direct current electrode negative (DCEN) **[40]**. About two-thirds of the total heat energy generated is concentrated on the wire. Therefore, in comparison with the case of utilizing the direct current reverse polarity (DCRP), higher melting rate and thus higher deposition rate of the wire are obtained. Consequently, the welding speed is higher, the shrinkage stresses resulted are less severe and hence the workpiece is less prone to distortion. The penetration, for the same reason, will be shallow and narrower **[41,42]**.

2. Reverse Polarity:

With this polarity, the current flows from the wire connected with the positive terminal of the power supply to the workpiece negatively charged. So, this polarity is also called direct current electrode positive (DCEP) **[40]**. About two-thirds of the total heat energy generated is concentrated on the workpiece. Therefore, the use of the DCRP results in a deeper penetration compared with the use of the DCSP or the AC for the same welding current value. The amount of the welding current is however considered the main determinant of the extent of penetration **[43]**.

2.8.4 Advantages of MIG Welding Method

1. Much faster than GTAW and shielded metal arc welding (SMAW).

2. Thick and thin workpieces can be welded efficiently.

3. It can be easily automated, and high deposition rates can be obtained.

4. This method uses no flux, and it is possible to obtain clean, smooth and spatter free welded surfaces, which helps reduce the overall welding cost.

5. The higher arc travel speed associated with this method reduces weld distortion **[44]**.

2.8.5 Disadvantages of MIG Welding Method

1. This method is slightly more complicated than GTAW and SMAW methods due to the variables that must be controlled well to get satisfactory welding results such as welding torch angle and manipulation (in semi-automatic welding), adjusting wire feeding speed, gas flow rate, and others.

2. Welding equipment is more complex, more expensive and less portable.

3. It does not work well when welding outdoors due to air currents drawing in covering gases.

4. Weld metal cooling rates are higher than in welding methods that deposit slag on the weld metal **[45]**.

2.8.6 Applications of MIG Welding Method

1. It can be used for welding carbon and silicon steels, low-alloy steels, stainless steels, dies and tool steels, aluminum, magnesium, copper, nickel and their alloys.

2. The manufacture of light industries such as refrigerator parts.

3. It can be successfully used in the aircraft, automotive and pressure vessel industries, and in shipbuilding **[46]**.

2.8.7 Parameters of MIG Welding Method

Due to the flexibility of welding process parameters, the MIG process is able to produce high quality weld joints for various applications. The most common MIG process parameters are type and diameter of the wire

electrode, welding current, wire feed rate, welding travel speed, composition and flow rate of the covering gas, and welding position **[47]**.

2.8.8 Wires Used with MIG Welding of Low Alloy Steel

The chemical composition of the wire used depends on the type of metal to be welded. Alloying elements may be added to the weld joint via welding wire. Steel welding wires are generally covered with copper in order to prevent rust and to increase the electrical conductivity **[48]**.

2.8.9 Classification of Wires Used for MIG Welding of Low Alloy Steel

The classification below shows how to identify the type of wire used for welding low alloy steels according to the American Welding Society (AWS) **[49]**.

ERXXS-X

E: a letter refers to electrode.

R: a letter refers to rod.

XX: numbers indicates the minimum tensile strength of the weld metal deposited. If they are 70 for example, this means that the minimum tensile strength of the weld metal is 70000 psi (Pounds per square inch), and so on.

S: a letter refers to solid wire.

X: defines the chemical properties, chemistry, amount of deoxidizers (Si, Mn, Al, Zr, Ti)

AWS A5.18 ER70S-6, ER80S-G, ER80S-Ni2 and ER100S-G are some of the most common wires used for welding low alloy steels **[49,50]**:

2.9 Weldability of Low Alloy Steels

The weldability of low alloy steel depends essentially on its hardenability, which in turn, depends largely on its chemical composition, mainly the carbon content. Other alloying elements such as manganese,

molybdenum, chromium, vanadium, nickel and silicon also have effects on the hardenability of low alloy steels, but with a much less extent **[51]**. Thickness and weld pool design are also important factors when considering weldability. Alloying elements, along with carbon, are all generally expressed as a single value called carbon equivalent (CE) **[52]**. The higher the carbon equivalent, the higher the hardenability which is closely related to weldability, the more difficult the steel is to weld and the steel becomes more prone to cracking **[53]**. Care and caution in addition to using special welding procedures should also be taken **[54,55]**.

Low alloy steels can be welded by the MIG process, however, high hardness and brittleness may occur in the weld zone and the heat effected zone (HAZ). The welding conditions should be low in hydrogen as well to obtain the best possible results when using this process **[39]**.

In order to have a high toughness in the weld zone when welding these steels, the austenitic stainless steel wires are sometimes used, however, the HAZ might remain hard and brittle. Therefore, it is important to use the preheating and postheating for avoiding the high hardness and brittleness of these zones **[39]**.

The need for preheating or/and postheating can be roughly determined for each type of steels via calculating the carbon equivalent, which is typically defined by several formulas. The following formula is usually used in most ASME applications:

$$CE = C+(Mn+Si)/6+(Cr+Mo+V)/5+(Ni+Cu)/15 \quad \text{Eq. (1)} \quad \textbf{[53]}$$

According to this formula, if the CE value is of 0.45 or less, steels can be welded without any preheating or postheating. The welding conditions should also be low in hydrogen. With higher CE values, steels may require either preheating or postheating treatment in order to relief stresses and hence to avoid weld cracking **[53]**. CE is an approximate value since it only

related to the chemical composition of the steel, as other factors like section thickness and joint constraints, which have a higher or equal effect on the weldability, are not taken into consideration. The cooling rate and thus the possibility of welding cracks can be reduced by some developments, which are carried out through the welding procedures. For example, a large V-shaped weld joint design with the use of a multi-pass welding process, in which the weld metal of the latest pass is deposited, surrounded by the weld metal of the previous passes from both sides. The heating of the subsequence pass will act as a tempering treatment to the HAZ resulting from the weld bead deposition of the pervious pass.

2.10 Metallurgical Effects of the Weld Thermal Cycle Associated with the MIG Process

2.10.1 Transformations in the Weld Metal

Solidification is the first transformation that occurs in the weld metal. The solidification mechanism of metals is summarized through nucleation and grain growth, as in the case of solidification that occurs in castings. In fusion welding, the formation of nuclei, usually, does not occur. This is because the molten metal (which its volume rarely exceeds one cubic inch) will solidify within a few seconds owing to very rapid cooling rate of the weld pool caused by the heat absorbed by the cold, relatively large sized base metal. The heat lost due to convection to the atmosphere is really another cause. This rapid cooling leads the weld metal to grow from the adjacent, incompletely melted grains of the base metal. Therefore, the growth mechanism in welding is important, whereas the nucleation is not **[48,56]**. The incompletely melted base metal grains serve as an ideal base from which the molten weld metal crystalizes. Hence, the grains of the molten weld metal will grow directly from the incompletely melted grains of the base metal, so that the grain boundaries of both

become continuous across the fusion line, as shown in Figure (2.4). Moreover, these grains are identical in the orientation of atoms.

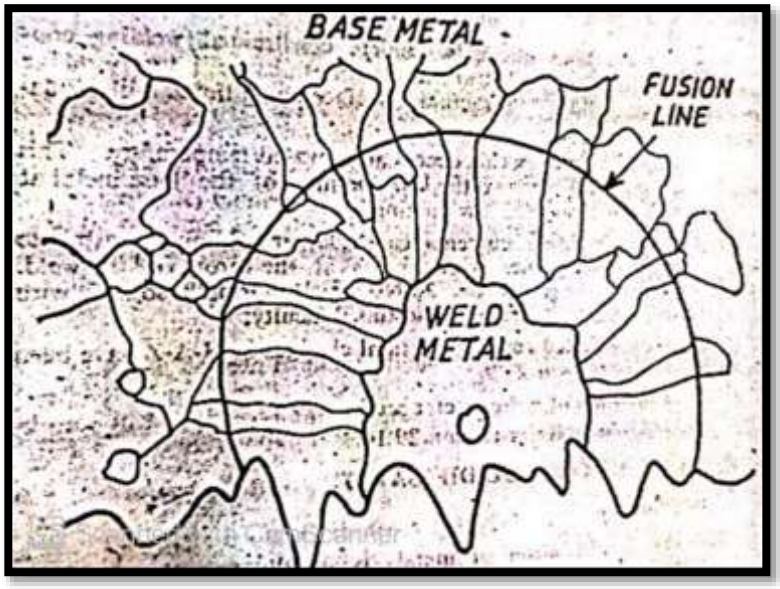

Figure (2.4): Weld metal growth [48].

In fusion welding, the existence of solid grains at the liquid-solid interface works as ready nuclei from which the granular growth releases **[48]**. In steels, the weld metal solidifies forming a solid solution of C, Mn and some other elements with iron. Based on cooling speed, the resulting grains might be dendritic or columnar. Heat typically flows from the weld zone towards the colder metal adjacent to this zone. The weld metal therefore, has columnar grains with right angles to the fusion line. This is what distinguishes grains resulting from single-pass welding. With multi-pass welding, and due to repeated heating, these grains transform into equiaxid grains, where each welding pass reheats the previous pass. This reduces the particle size of the formed grains, consequently improving the mechanical properties of the weld zone **[57]**.

The weld metal is a mixture of the filler metal with the molten base metal. The mixing of a portion of the base metal with the deposited filler metal is known as dilution process, which can be expressed as **[58]**:

$$\text{Dilution ratio (D) \%} = \frac{\text{weight of the molten base metal}}{\text{total weight of the molten metal}} * 100$$

The maximum dilution occurs in thin section butt-welding without beveling the edges with one-pass. Less dilution happens in the case of multi-pass welding, with edge preparation, as shown in Figure (2.5):

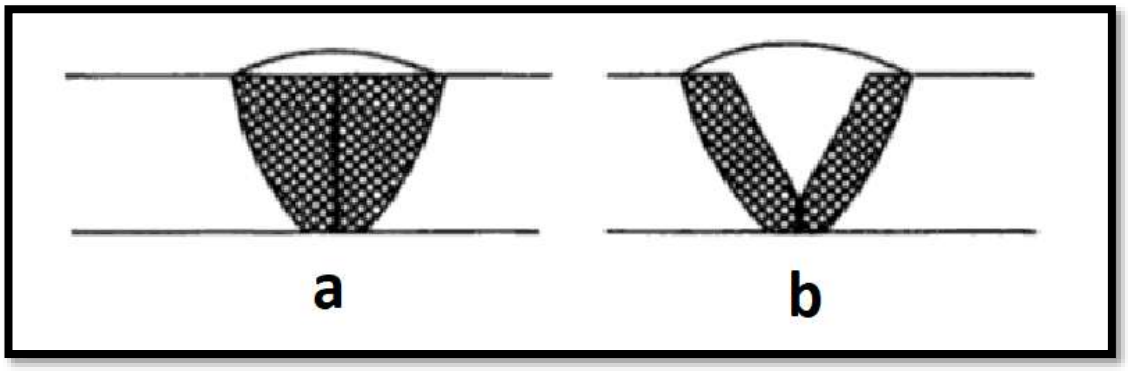

Figure (2.5): Dilution of the (a): one pass square butt joint weld (b): multi-pass single-V butt joint weld **[59]**.

It is worth mentioning that the first bead in the case of multi-pass welding, which is called root bead, smelts a large proportion of the base metal in comparison with the subsequent beads. Cracks possibly occur in the root bead, as this bead exhibits high hardness and brittleness due to the high dilution ratio, and excessive cooling caused by heat absorbing from this small-sized bead by the large size of the cold base metal. The large strain caused by shrinkage stresses also promotes the development of these cracks. Therefore, caution should be considered when welding the root pass, particularly in high carbon steels, to avoid cracks in this bead **[60]**.

Dilution is more prominent when welding dissimilar metals. It however can be decreased via depositing one or a number of weld layers on the edges of the joint being welded before the start of the welding process. This is called the buttering process, and in some cases, specific alloys can be used for this purpose **[58]**. Increasing the carbon content does not increase the weld metal strength as it does, e.g., with the wrought steel, because such an

increase causes segregation of carbon during the solidification. This leads to formation of cementite during the subsequent solid-state transformation of austenite, decreasing the toughness of the weld metal. Therefore, the carbon content in the weld metal should be kept low as (0.1%) as a maximum. This ratio should therefore not be exceeded in the welding electrodes, whatever the strength desired of the weld metal, or the carbon content in the base metal. When the carbon content of the weld metal is maintained low, the microstructure will mostly be a mixture of ferrite and carbides with a very small proportion of bainite or martensite**[58]**.

2.10.2 Thermal Effects of the MIG Welding Process on the Base Metal

The base metal adjacent to the weld zone is typically divided into two zones: the HAZ and the base metal unaffected by heat **[48]**.

2.10.2.1 Heat Affected Zone

It is the region adjacent to the weld zone, which represents the base metal that is not melted by the welding heat, but is heated to a temperature and for a period sufficient for grain growth to occur. This region undergoes complex thermal cycles of sudden heating to various temperatures, ranged from the melting temperature to that of the unaffected base metal. The heating is then followed by rapid cooling due to the nearby cold metal and the surrounding atmosphere. This heating and cooling cycle acts as various heat treatments for each region of the HAZ. This zone therefore consists of a series of structures, gradient and different in their mechanical properties. In low alloy steels, these structures might vary from the hard martensite to the coarse pearlite. The HAZ width in arc welds doesn’t exceed a few millimeters.

When welding low alloy steels with a single pass by MIG process, three different metallurgical regions can be observed **[48]**:

A. Grain Growth Region: it is just adjacent to the fusion boundary (weld zone). In this region, the base metal is heated to temperatures in a range between above the upper critical temperature (A_3) and melting temperature (Figure 2.6). This resulted in coarsening the structure or grain growth **[48]**. The largest grain growth region and the maximum grain size occur as the cooling rate decreases. The cooling rate depends upon the amount of heat used during welding, initial temperature of the base metal, thickness of the welds in addition to the weld joint design. The high initial temperature of base metals and welding heat causes slow cooling rates, whereas the large weldment thicknesses result in rapid cooling rates. Generally, the cooling rate of this region is greater than those in the other regions of the HAZ, due to the severe thermal drop from the temperature of this region to that of the cold base metal **[48,56]**. This region is therefore the hardest HAZ region in low carbon steel welds **[61]**.

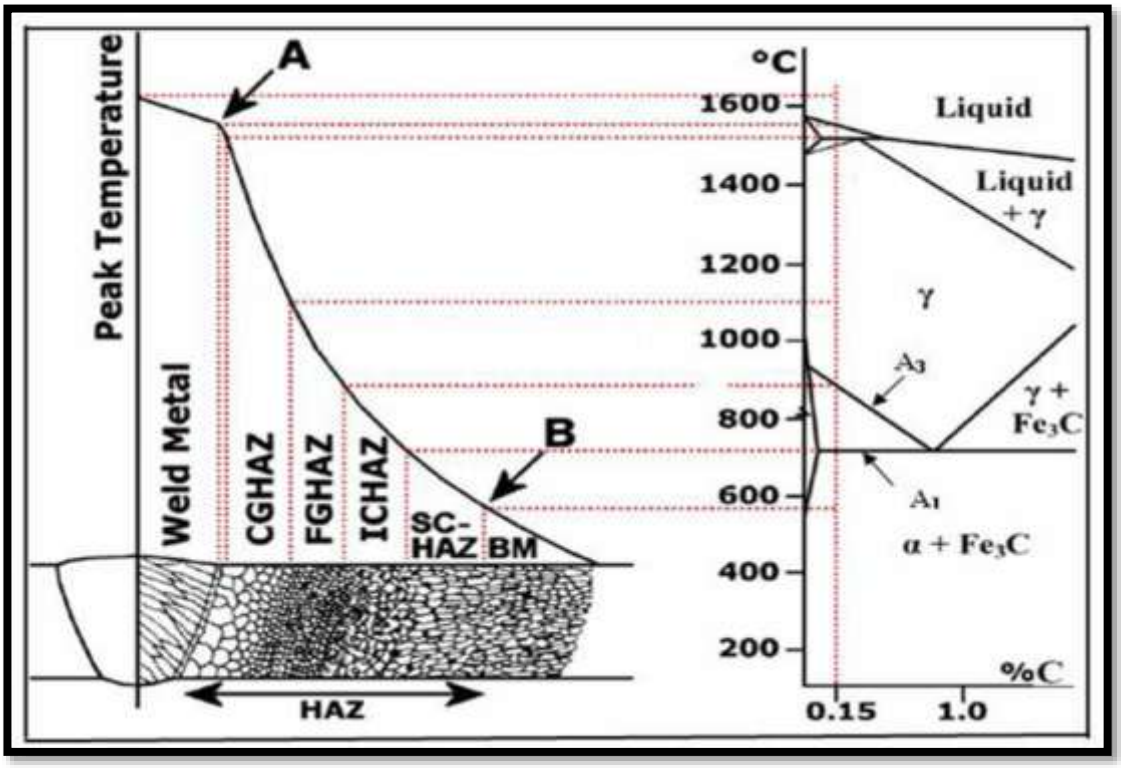

Figure (2.6): Fe-C phase diagram **[62]**.

The microstructure in this region is based on the percentage of carbon and alloying elements, grain size and cooling rate. For low carbon steel welds, the structure in the grain growth region is pro-eutectoid ferrite at the grain boundaries of the prior austenite, whereas the grains themselves are usually ferrite with pearlite, or ferrite with bainite. With increasing the cooling rate or the content of carbon and alloying elements, the ferrite grains disappear. The austenite grains then transform into upper or lower bainite, martensite or a mixture of these microstructures **[63]**. The resulting grain size depends on the grain size of the austenite. If the austenitic grains were large, the resulting structure will be coarse **[63]**. Generally, the metal in this region losses some of its ductility particularly the impact strength. Figure (2.7A) shows the structure of this region.

B. Grain Refined Region: it is the region adjacent to that of grain growth, at which the metal is heated to a temperature directly above A_3 **[48]**. The metal in this region completely transforms to a new, fine-grained austenitic structure, as the heating time is not long enough for the austenite grains to grow. Therefore, moderate cooling will form fine pearlitic grains. This is identical to the normalizing heat treatment applied to carbon steels, which includes heating to this temperature before cooling with still air **[64]**. This region has relatively high strength and toughness, the same features and properties of normalized steels. Figure (2.7B) shows the structure of this region, where dark areas indicate pearlite and light areas indicate ferrite.

C. Transition Region: during welding, this region is exposed to temperatures between A_3 and the lower critical temperature (A_1) **[48]**. This heating transforms pearlite (partially at least) into fine-grained austenite, but it is not sufficient to transform ferrite grains **[54]**. A partial allotropic recrystallization occurs in this region. Upon cooling, the fine austenite grains transform into fine pearlite. Obviously, in this case, the pearlite

grains are refined while the ferrite grains remain the same **[48]**. Figure (2.7C) represents the microstructure of this region.

For alloy steels, this region is of particular interest, as the same cooling rate might be enough to convert the fine grains of austenite to martensite, resulting in high hardness and brittleness in this region. This exposes these kinds of steels to hydrogen cracks. It should be noted that the main reason for the formation of martensite in this region is carbon, where with the increase in the percentage of carbon and other alloying elements, the hardenability of steels increases as mentioned earlier.

2.10.2.2 Unaffected Base Metal

The base metal that is heated upon welding to temperatures insufficient to make change in its structure, comes directly after the HAZ **[48]**. Figure (2.7D) shows the microstructure of the base metal of low carbon steel unaffected by welding heat.

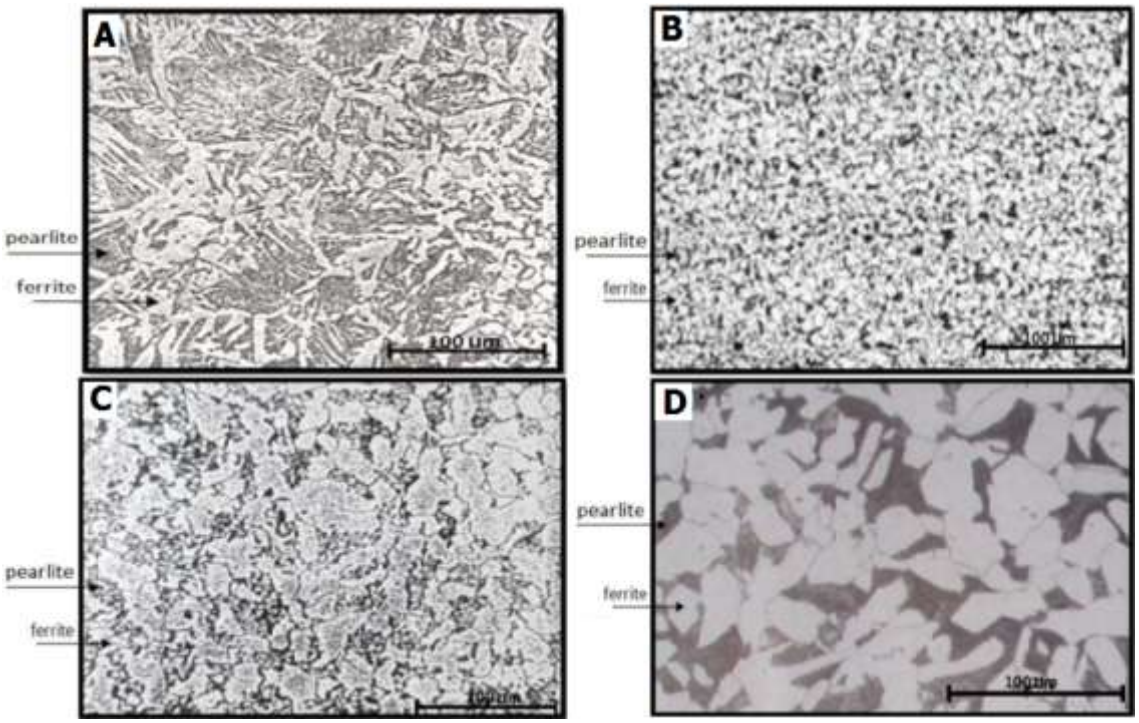

Figure (2.7): Microstructure of the (A): grain growth region, (B): grain refined region, (C): transition region and (D): base metal of low carbon steel unaffected by heat **[48]**.

2.11 Extraordinary Processing Technology of Wire Arc Additive Manufacturing

At present, the forming process of WAAM is continually optimized to improve the microstructure and properties. The auxiliary process is not only necessary for heat treatment, but also includes extraordinary processes like adding suitable alloy powder, laser and the forging **[65].**

2.11.1 Adding Suitable Alloy Powder

When the powder is added during the WAAM, the grains of the intermediate layer change from columnar to fine equiaxed, and promotes the grain refinement of alloy. Therefore, the mechanical properties of the WAAM alloy show more isotropy in both directions; the ultimate tensile strength and the microhardness of the intermediate layer increase **[65].**

2.11.2 Addition of a Laser

Adding a laser during the WAAM process shows that the laser can significantly make the molten pool more stable (average fluctuation is reduced by more than 35%). The surface of the previous layer will be smoother with improving the accuracy of the WAAM **[66]**. Figure (2.8) shows a schematic of this method.

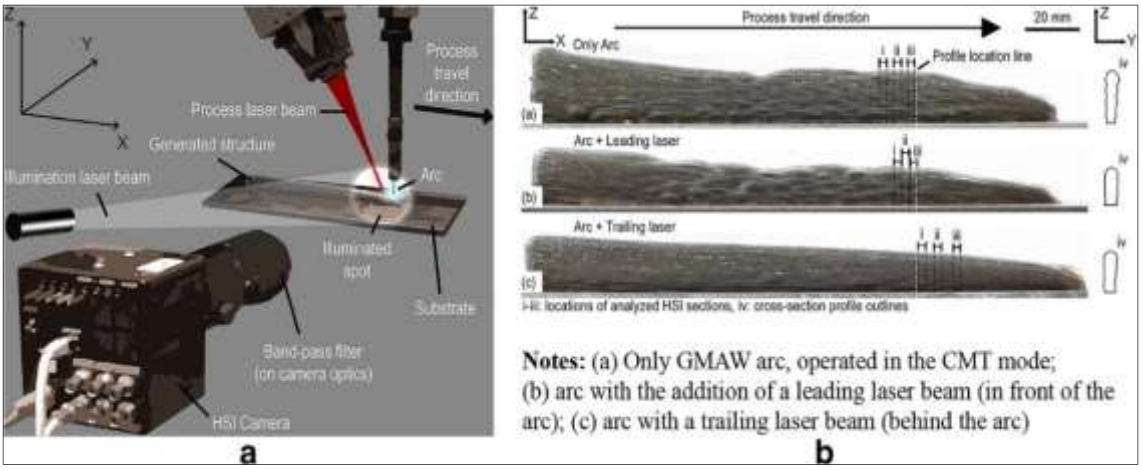

Figure (2.8): (a): WAAM with laser beams and illumination laser spot over the process zone (b): macrographs of generated walls using different WAAM technologies **[66]**.

2.11.3 The Ultrasonic Micro-Forging

This method consists of forming WAAM workpieces and forging after deposition. The combination of forging and WAAM can be during WAAM formation or it can be processed after WAAM formation **[67]**. The design of the machine is shown in Figure (2.9). The material is locally forged immediately after deposition, and in-situ viscoplastic deformation occurs at high temperatures. In the subsequent layer deposition, recrystallization of the previously solidified structure occurs, thus refining the microstructure. The mechanical properties of WAAM materials can be greatly improved by hot forging **[68].**

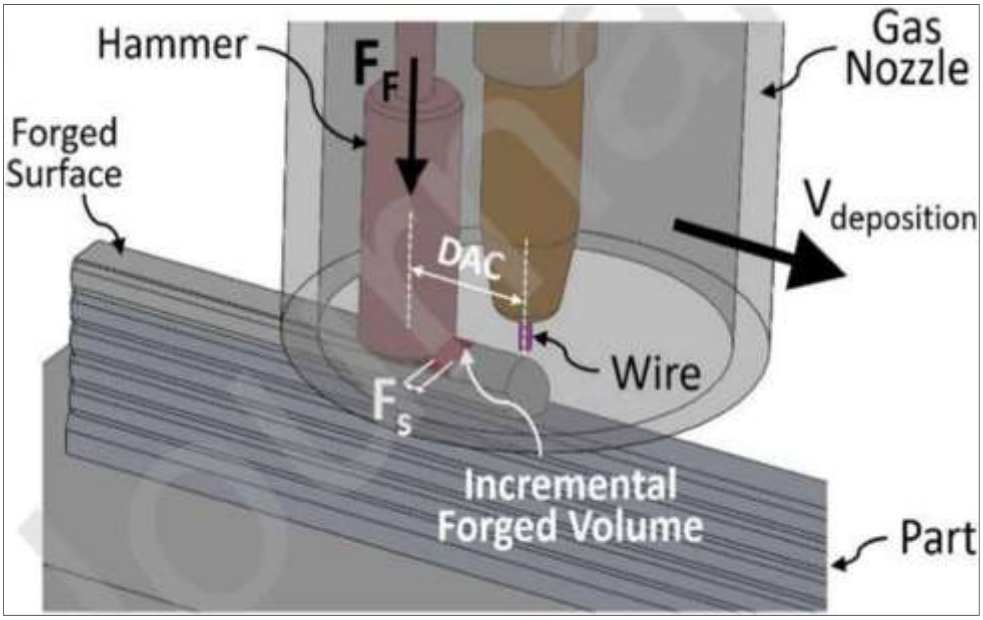

Figure (2.9): Isometric view (3D) of a schematic representation of the forged area at each step **[67].**

2.12 Forging Process

Forging is a deformation process where the workpiece is compressed between two dies, using either impact or gradual pressure to form the part. Forging process produces parts of superior mechanical properties with minimal material wastage. The starting material in this process has a relatively simple geometry; this material is plastically deformed into a

product of relatively complex configuration in one or more operations. While the forging process gives superior product quality compared to other manufacturing processes, there are some defects that will come slightly if proper care is not taken in the design of the forging processes. There are many imperfections that can be considered defects, ranging from those traceable to starting materials to those caused by one of the forging or post-forging processes **[69]**.

2.12.1 Classification of Forging Processes

There are a large number of forging processes that can be classified by workpiece temperature, by die arrangements, or by machine **[70]**. The most important classification of the above is the first category, on which will be focused.

a) Hot forging (most widely used): Forging is carried out at a temperature above the recrystallization temperature of the metal. The recrystallization temperature is defined as the temperature at which new grains are formed in the metal. This kind of extreme heat is necessary to avoid strain hardening of the metal during deformation **[69]**.

Advantages: High strain rates and hence easy metal flow, recrystallization and recovery are possible and the forces required are less **[71]**.

Disadvantages: Lubrication is difficult at high temperatures; oxidation and scaling occur on the workpiece, poor surface finish, less precise tolerances, and possible warping of the material during the cooling process **[71]**.

b) Cold forging: Forging is carried out at or near room temperature (below the recrystallization temp.) of the metal. Carbon and standard alloy steels are most commonly cold-forged. Cold forging is generally preferred as the metal is already soft, like aluminum. This process is usually less expensive than hot forging and the end product requires little or no finishing work. Cold forging is also less susceptible to contamination problems, and the final component has an overall better surface finish **[69]**.

Advantages: Production rates are very high with special die life, improves mechanical properties, less friction between die surface and workpiece, lubrication is easy, and there is no oxidation or scaling on the work **[69,71]**.

Disadvantages: Residual stresses may occur, heavier and more powerful equipment is needed, stronger tooling is required, and tool design and manufacturing are critical **[69]**.

c) Warm forging: The temperature range for the warm forging of steel runs from above room temperature to below the recrystallization temperature. Compared with cold forging, warm forging has the potential advantages of: reduced tooling loads, reduced press loads, increased steel ductility, elimination of need to anneal prior to forging, and favorable as-forged properties that can eliminate heat treatment. In warm forging, the billet is heated below the recrystallization temperature, up to 700 to 800 °C for steels, in order to lower the flow stress and the forging pressures **[69]**.

Advantages: High production rates, excellent dimensional tolerances and surface finish of forged parts, important savings in material and machining, favorable grain flow to improve strength, greater toughness of the forged part **[69,70]**.

Disadvantages: Short die life, strict material temperature control and low forming accuracy compared to cold forging, preventing its tremendously widespread use **[72]**.

2.12.2 Selection of Forging Machine

The selection of the forging machine depends on the requirements of force and energy, the material to be forged (soft material-using press, hard material-using hammers), the size and complexity of forging, the strength of the workpiece material, the sensitivity of the material to the deformation rate, the rate of output, the dimensional precision, the maintenance, the degree of operation required, the level of noise and the cost **[73]**.

2.12.3 Characteristics of Forging

Typically includes separate parts, can be used on hot or cold materials, sometimes requires additional finishing processes such as heat treatment, machining or washing, can be performed at rapid or slow deformation levels, can be used for very small or very large parts, and improves the physical properties of a component by monitoring and refining the flow of materials or grains **[74,73].**

2.12.4 Common Applications of Forging

Automotive passenger cars, trucks, buses, trailers, motorcycles and bicycles. Bearings, ball and roller. Electric power generation/transmission. Industrial and commercial machinery and equipment. Hand tools. Industrial tools. Mechanical power transmission equipment. Internal combustion engines. Oil field machinery and equipment. Off highway, equipment (construction, mining and materials handling). Pipeline fittings. Plumbing fixtures, valves and fittings. Pumps and compressors. Railroad equipment and spikes **[75]**.

2.13 Advantages of Additive Manufacturing

The ability to create complicated geometries that cannot be made by traditional manufacturing methods, as well as the lack of auxiliary devices and tools, are fundamental benefits of AM procedures. From a business sense, these benefits have numerous important consequences. Individual components are frequently fabricated in separate factories using specialized tools before being sent to assembly sites. Parts are created without the use of specialist tools, allowing for on-site production of a large number of parts and the removal of supply chains. Furthermore, because AM can print interlocking pieces, it reduces the amount of parts per component and

eliminates the need for assembly. In terms of product distribution, AM has the potential to drastically alter the things that are dispersed. AM products are arguably based on the product model's digital file; thus, the file rather than the physical product could be distributed. Any individual having access to the right AM machinery could create the physical product using a digital file **[76]**. From a logistical aspect, AM allows manufacturers to make parts on an as-needed basis for items that aren't purchased frequently but must be warehoused otherwise, decreasing warehouse load. Because of the potential of additive manufacturing, these parts might be produced in much lower amounts, lowering the expense of storing many uncommon replacement parts. Because AM methods may be used to manufacture specific parts, various effective uses of AM technology can already be found, including custom orthodontics, hearing aids, prostheses, and other medical devices **[77].**

2.14 Limitations of Additive Manufacturing

It is vital to remember that the AM advantages come with problems. The following are some of the key obstacles to AM adoption **[78]**:

1. There is a scarcity of material variety.

2. Concerns about intellectual property.

3. In AM there is a scarcity of experienced designers and engineers.

4. Post-processing of AM components is required.

5. Additional norms and regulations for the AM and parts are required.

6. While AM can help supply chains become more nimble and reduce logistics costs, it can also lead to higher production costs and a lack of economies of scale.

7. Even as supply chain complexity diminishes, AM adoption will necessitate complicated testing and quality assurance methods, resulting in downstream supply chain complexity.

8. In the case of complex applications, AM techniques still require quality and accuracy enhancements.

9. It is also vital to keep in mind that, like traditional manufacturing processes, products made by AM are prone to flaws **[79].**

2.15 Applications of Additive Manufacturing

Industrial applications of AM technologies have evolved at a rapid rate since their introduction, integrating into interdisciplinary disciplines of science and engineering. AM technologies are now used in a wide range of applications such as automotive manufacturers, machine tool industry, aerospace companies, medicinal industries, construction and architectural industries, jewellery, printed Food and textiles [**9]**.

2.16 Literature Review

The literature review provides detailed information on researches dealing with the microstructure and mechanical properties of steels produced by the WAAM.

In 2019, Ron et al. [80] evaluated the environmental behavior of low carbon steel deposited by the WAAM using 1.2 mm of ER70S-6 steel wire on a counterpart wrought steel alloy ASTM (A36). The welding process was carried out using a welding manipulator composed of a welding robot integrated with a numerically controlled computer. The welding process parameters included a wire feed rate (WFR) of 6.1 m/min, an electrical current of 210 A, a voltage of 23.9 V, and the protective gas atmosphere for the metal arc welding process consisted of 98% argon and 2% oxygen. The microscopy showed a reduced amount of secondary pearlite colonies and the predominant phase was ferrite; A36 alloy presented a regular ferrite matrix and a secondary pearlite colonies. A minor amount of retained austenite was also included in the ferrite matrix in both alloys. Hardness

(HV) of the printed alloy was 192.4 and of its reference (A36 alloy) was 259.1. Tensile strength was 475.7 MPa and 611.2 MPa respectively, and total elongation (%) was 34.6 and 12.6 respectively. The findings revealed that the tensile strength and hardness of the printed alloy were relatively reduced, as compared to the reference A36 alloy. In parallel, the ductility in terms of elongation percent was significantly increased.

In 2019, Waqas et al. [81] studied the directional tensile properties of a layer-by-layer built steel structure using a robot-assisted GMAW additive manufacturing. An ER70S-6 welding electrode was used for stacking the layers to create a thin wall structure. Tensile specimens were taken parallel and perpendicular to the deposition direction as well as at different layer levels. The results showed that the resulting structure has directional characteristics with better tensile strength and ductility for the specimens taken parallel to the deposition direction as compared to the specimens taken perpendicularly. The least tensile strength obtained by this process was comparable to the AISI 1008 low carbon steel with similar carbon content, so it can be used as an alternative.

Rafieazad et al. in 2019 [82] investigated a low-carbon low-alloy steel wall built by the WAAM method using a GMAW torch translated by a six-axis robotic arm. The base plate was ASTM A36 mild steel, and 0.8 mm diameter ER70S-6 wire was used as feedstock material. The process was carried out using an arc current of 320 A, an arc voltage of 28 V, a WFR of 104 mm/s, a scan rate of 5 mm/s, and pure argon as a shielding gas with a flow rate of 45 l/min. The dominant microstructure of the fabricated part contained randomly oriented fine polygonal ferrite and a low volume fraction of lamellar pearlite as primary micro-constituents. Additionally, a small content of bainite and acicular ferrite were also detected along the melt-pool boundaries, where the material undergoes a faster cooling rate during solidification in comparison with the center of the melt pool. The

average micro-hardness of the WAAM-fabricated component was 160 HV, the highest micro-hardness value reached 175 HV and the lowest was 150 HV. Mechanical properties of the part studied at different orientations relative to the building direction, revealed a comparable tensile strength along the deposition (horizontal) direction and the building (vertical) direction of the fabricated part (~ 400 MPa and ~ 500 MPa for the yield and ultimate tensile strengths, respectively). However, the plastic tensile strain obtained at failure along the horizontal direction was nearly three times higher than that of the vertical direction implying some extent of anisotropy in ductility.

In 2020, Valdemar et al. [83] studied a new variant of WAAM based on hot forging. During WAAM, the material is locally forged immediately after deposition, and in-situ, at high temperatures, viscoplastic deformation occurs. AISI316L stainless steel wire with a diameter of 1 mm was used as a feedstock material deposited on a mild steel substrate. In the subsequent layer deposition, recrystallization of the previous solidification structure occurs that refines the microstructure. Because of its similarity with hot forging, this variant was named HF-WAAM. Forging forces of 17 N and 55 N were applied to plastically deform the material. The results showed that this new variant refines the solidification microstructure. Mechanical characterization was performed and improvements on both yield strength (YS) and ultimate tensile strength (UTS) were achieved. Compared to as build part, the YS increased from 360 to 450 MPa, UTS improved from 574 to 622 MPa, while elongation to fracture reduced from 32 to 28 %.

In 2020, Le and Paris [84] studied the microstructures and mechanical properties of gas-metal-arc-welding additive manufacturing (GMAWAM) for the repurposing of components. This method used two low-carbon steel (ASTM A36) plates as existing components to build the test specimens. ER70S-6 welding wire with a diameter of 1.2 mm was used to build new

features (i.e., thin walls) on the substrates; CO_2 gas was employed for the shielding purpose during the welding process. Welding variants including welding torch travel speed of 300 mm/min, welding current of 90 A, and voltage of 18 V were used. A new thin-walled feature was built on the first plate to investigate the microstructure and hardness of materials. The second plate was used to build another thin-walled for preparing the tensile test specimens. The results showed that the new thin walls built by GMAWAM possess different microstructures. The upper region of thin-walled features exhibited lamellar structures, the middle region was characterized by granular structures, and mixed equiaxed and lamellar grains appeared in the bottom region. The middle region is the softest with an average hardness value of (176 HV), followed by the bottom region (195 HV) and the top region (205 HV). This result is coherent with specimen microstructures. Tensile test showed that the YS and UTS of the resulting steel walls were normally higher than those of the wrought ASTM A36 steel (YS of 250 MPa and UTS of 400–550 MPa), indicating better material properties achieved using GMAWAM vs. conventional manufacturing processes.

Aldalur et al. studied **in 2020 [85]** the effect of oscillatory and overlapping deposition strategies on microstructure and mechanical properties. The WAAM technique, based on GMAW, was used to manufacture walls with different strategies by the commercially produced ER70S-6 mild steel wire with a 1.2 mm diameter. ASTM A36 steel plates were used as a substrate. For the experiments, an automatic welding system was used with a WFR of 8 m/min, a current of 229 A, a voltage of 27.1V and a single bead thickness of 8 mm. The test samples were two walls created using two different deposition strategies: Wall 1 overlapping and Wall 2 oscillating. Microscopy of the overlapped wall showed that each deposited bead was clearly observed, and a heterogeneous microstructure was obtained with

intercalated areas of polygonal ferrite and acicular ferrite. This acicular ferrite appeared in areas where the heat input of the next layer does not affect, such as the last layer deposited at the top of the wall. In the oscillated wall, the acicular ferrite also appeared in the last layer. In the remainder of the wall, layer bands were observed, and a homogeneous polygonal ferrite microstructure was obtained. In this case, the grain size was larger than in the overlapped wall due to the heat accumulation suffered. The hardness and microstructure were closely related properties. As a result, higher values of hardness HV were obtained at the top part of overlapped and oscillated walls (163 and 154 respectively). The overlapped wall hardness values were greater than the oscillated one because of the heterogeneity in the microstructure. Isotropic mechanical properties were achieved in both manufactured walls; namely, in the vertical and horizontal directions, the mechanical properties were similar. Moreover, in the overlapped wall, UTS and YS values (498 and 368 respectively) were greater than the oscillated values (478 and 354 respectively) because of the smaller grain size obtained. This was a good example of a fine-grain strengthening mechanism.

In 2020, Rodrigues et al. [86] studied the impact of different heat inputs on the thermal behavior, microstructural evolution and mechanical properties of a HSLA steel part produced by WAAM. The feedstock material was 1mm diameter ER110S-G HSLA steel wire deposited onto a mild steel substrate using GMAW technique. The travel speed was 5 mm/s, voltage 19 V and flow rate 16 l/min (99.999% Ar). Between the deposited layers, SiC particles with a grain size of 1 to 2 μm, were added. The results were used as a criterion to evaluate the effect of SiC inoculation during WAAM. Microscopy revealed the presence of a more homogenous microstructure in the sample inoculated with SiC particles. Near isotropic grains formed upon the introduction of SiC into the molten pool. The

dissociation of the SiC particles in the molten pool led to an increased carbon content in austenite, which resulted in the coexistence of bainite, retained austenite (M-A) and Fe_3C. The hardness increased, on average, from 290 up to 426 HV. The tensile strength of the SiC-inoculated samples was significantly improved compared to the non-inoculated ones. This increase was attributed to the refined grain structure, higher carbon content, retained austenite, and Fe_3C precipitation in the inoculated samples.

In 2021, Pattarawadee et al. [87] evaluated the forming characteristics of single-pass MIG welding deposit for multi-layer additive manufacturing parts. Influences of arc current, arc voltage, arc distances, welding speed, wire feed speed, temperatures and heat input on layer formation were analyzed. The deposition of material by MIG process was controlled by a robot controller for constructing walls of rectangular box shape. A single weld line wall was deposited on a 12 mm thick ASTM A36 low carbon steel plate using a mild steel wire grade ER70S-6 (1.2 mm diameter) as a filler metal. The process was operated at 18.5 V and WFR 2.4 m/min, shielding gas was CO_2. It was found that the average micro-hardness at the top, the middle, and the bottom regions was in similar value (155.80, 151.70, 155.60 HV, respectively), and the tensile strength values were 472.71-491.12 MPa according to transverse and longitudinal sections of the specimens.

2.16.1 Summary of Literature Reviewed

The most reviewed literature related to the current study is summarised in Table (2.2).

Table (2.2): Summary of literature reviewed.

I	Researchers	Shielding Gas	Substrate	Additive Material	Major Results
1	Pattaraw-adee et al. 2021	CO_2	ASTM A36 mild steel	ER70S-6 wire (1.2mm)	Micro-hardness values were 151.7-155.8 HV, and the tensile strength values were 472.71-491.12 MPa based on transverse and longitudinal sections of the specimens.
2	Valdemar et al. 2020	Pure Ar	Mild steel	AISI316L stainless steel wire (1mm)	A new variant of WAAM based on hot forging of the material immediately after deposition was investigated to refine the solidified microstructure. Compared to as build part, the YS increased from 360 to 450 MPa, UTS improved from 574 to 622 MPa, while elongation to fracture reduced from 32 to 28 %.
3	Rafieazad et al. 2019	Pure Ar	ASTM A36 mild steel	ER70S-6 wire (0.8mm)	The dominant structure of the fabricated part contained randomly oriented fine polygonal ferrite and a low amount of lamellar pearlite. Small contents of bainite and acicular ferrite were also detected along the melt pool boundaries. The highest micro-hardness value reached 175 HV and the lowest was 150 HV. A similar tensile strength (~ 500 MPa) along the deposition (horizontal) direction and the building (vertical) direction of the part was revealed. The ductility along the horizontal direction was nearly three times higher than that of the vertical direction.
4	Ron et al. 2019	98% Ar and 2% O_2	Wrought steel alloy ASTM A36	ER70S-6 wire (1.2mm)	Microscopy of the additive L.C.S revealed a reduced amount of pearlite; the reference ST-37 alloy presented a regular ferrite matrix with pearlite phase. Hardness (HV) of the printed alloy was 192.4 and that of its reference alloy was 259.1. Tensile strength was 475.7 MPa and 611.2 MPa respectively, and total elongation (%) was 34.6 and 12.6 respectively.
5	Waqas et al. 2019	-----	-------	ER70S-6 wire	The resulting structure had directional characteristics with better tensile strength and ductility for specimens taken parallel to the deposition direction as compared to those taken perpendicularly.

It is clearly noted from the review of previous literatures and Table (2.2) that there are some researches that dealt with the microstructure and mechanical properties of mild steel produced by the WAAM process. Most of them were however on mild steel substrates and only one on high strength low alloy steel. As of this writing, no research has been found by the auther dealing with the study of the microstructure and mechanical properties of a steel-based material deposited on a low alloy steel substrate using gas metal arc additive manufacturing. Moreover, no research was found in the previous literature dealing with steel produced by the WAAM process along with the forging process, except for one study based on combining WAAM with hot forging of AISI316L stainless steel. In addition, there has been no research examining the effect of using a wide variety of deposition patterns and cold forging on the microstructure and mechanical properties of steel-based materials built on a low alloy steel substrate by the WAAM.

CHAPTER THREE:

EXPERIMENTAL PART

EXPERIMENTAL PART

3.1 Introduction

The chapter provides a clear vision on the experimental work and describes all the conditions under which the tests have been carried out. It includes materials and equipment used for wire arc additive manufacturing and forging process. Mechanical properties of the produced samples were examined by micro-hardness and tensile tests. Changes in the samples microstructure were evaluated by optical microscopy (OM), scanning electron microscopy (SEM) and energy dispersive spectrometry (EDS). Figure (3.1) shows the general program outline used in the current work.

3.2 Materials and their Specifications

3.2.1 The Substrate used in this Study

The chemical composition of the low alloy steel plates used in this study as substrates according to the American Iron and Steel Institute (AISI) **[88]** is shown in Table (3.1). The cross section of the plate is (9*70) mm, knowing that the raw material is annealed. The pieces (substrates) were prepared from the raw material with a length of (100mm) for each piece. The chemical composition analysis for the raw material was carried out using Spectro Max Metal Analyzer at the State Company for Engineering Rehabilitation and Testing–Baghdad. Table (3.1) shows the chemical composition (with an average of three readings) of the raw material used as a substrate. It falls within the range of the chemical composition according to AISI (nominal).

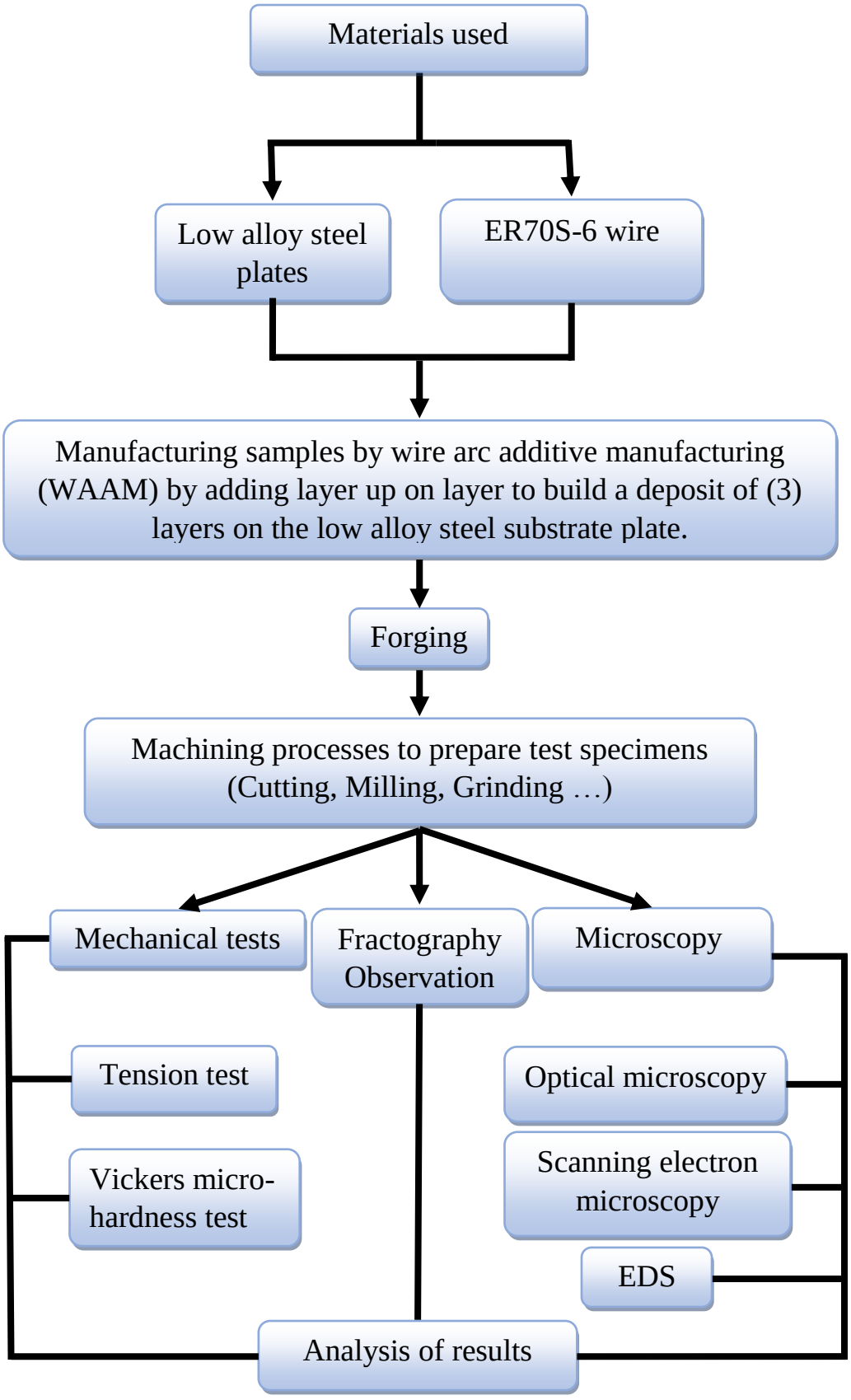

Figure (3.1): Flowchart of the present work.

Table (3.1): Specifications of the alloy used in the research [89].

Alloy		Chemical composition (wt. %)						tensile strength (MPa)	Vickers hardness (HV)	Spec. symbol (AISI)
		C	Mn	Si	Cr	P	S			
Low alloy steel	Nominal	0.51-0.59	0.7-0.9	0.15-0.3	0.7-0.9	0.04 max.	0.04 max.	680 min.	220	5155
	Actual	0.533	0.764	0.258	0.863	0.0119	0.0069	696	265	

3.2.2 Solid Wire used in this Work

Table (3.2) shows specifications of the MIG welding wire used as a filler metal according to American Welding Society (AWS) A5.18 **[90]**.

Table (3.2): Solid wire specifications

Copper coated steel wire	Wire diameter (mm)	Typical properties all weld metal			Typical chemical composition of wire (wt.%)			
		Tensile strength (MPa)	**Yield stress (MPa)**	**El. (%)**	**C**	**Mn**	**Si**	**Fe**
ER70S -6	1	540	440	30	0.08	1.5	0.85	Balance

3.4 Experimental Procedure

3.4.1 Wire Arc Additive Manufacturing Operation

Experiments were carried out using a semi-automated MIG welding system shown schematically in Figure (3.3) to build the samples. Lincoln Electric Power MIG (350MP) machine was utilized as a source of energy. The target was building three layers on the substrate with dimensions of (7×70×100) mm using ER70S-6 filler wire with a diameter of 1 mm as a feedstock material, and pure CO_2 as a shielding gas. A low alloy steel plate with dimensions of (9×70×100) mm was used as a substrate for building, as shown in Figure (3.4). The oxide layer on the surface of the substrate plate was removed by the use of a wire brush. The WAAM process was however carried out using the parameters shown in Table (3.3).

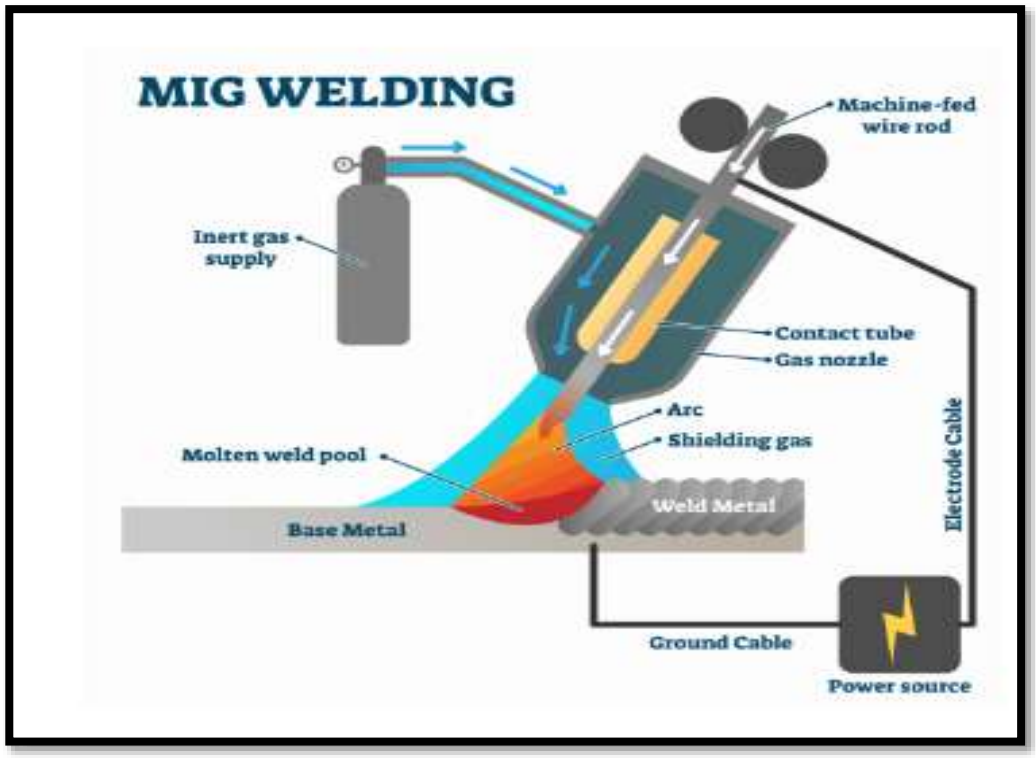

Figure (3.2): Schematic representation of the semi-automated MIG welding.

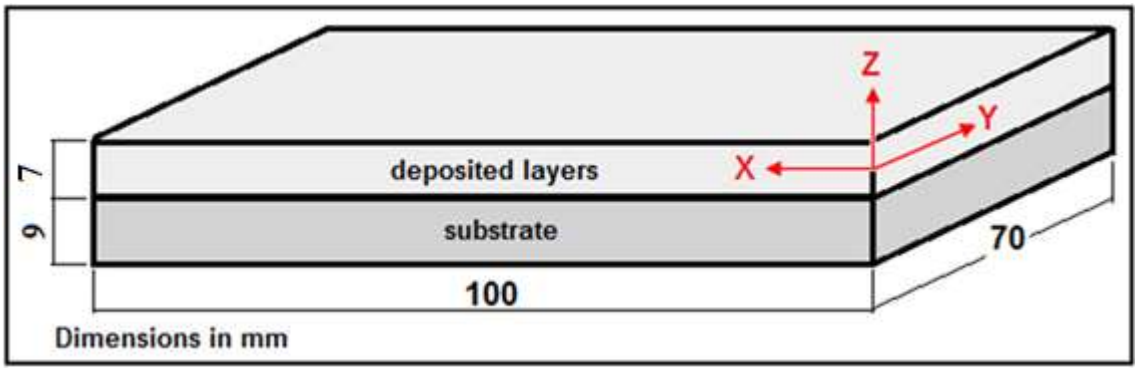

Figure (3.3): Deposited layers on the substrate.

Table (3.3): MIG parameters used with the WAAM process.

Welding current	130 A
Welding Voltage	21V
Wire feeding rate	5 m/min
Travel speed	120 mm/min
Shielding gas	pure CO_2
Gas flow rate	10 l/min
Bead type	Weaving bead
Bead width	8 mm

Fifteen samples were prepared using five different deposition patterns shown schematically in Figure (3.5). The first pattern was longitudinal, in a direction parallel to the X-axis of the substrate (Figure 3.4), the second pattern was transverse, in a direction parallel to the Y-axis, and the third pattern was a right network of sequentially longitudinal and transverse lines. The fourth deposition pattern was an oblique at an angle of 45°, while the last pattern was an oblique network at an angle of 45° as well.

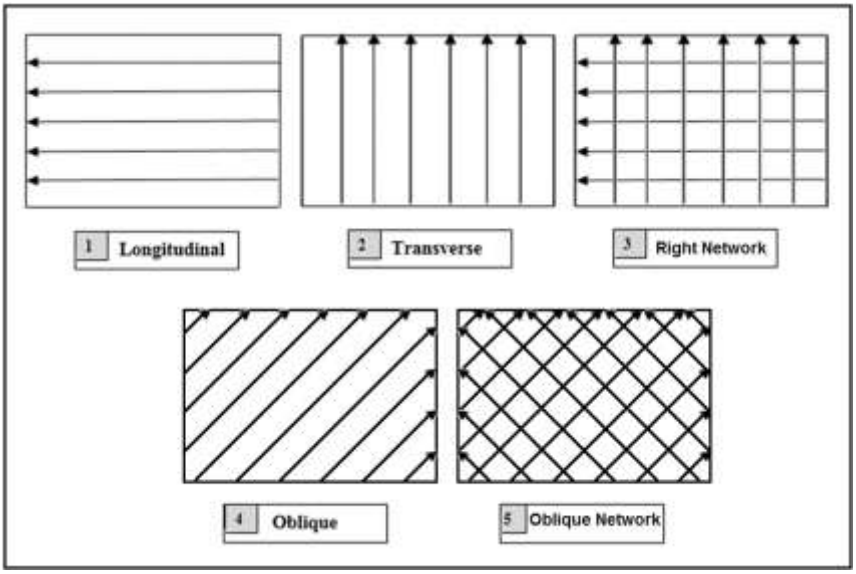

Figure (3.4): Deposition patterns of the WAAM.

Figure (3.5): WAAM samples with five different deposition patterns.

3.4.2 Forging Operation

The Forging process was open die cold forging schematically shown in Figure (3.7) using an electric forging hammer KALININ (MA-417). Ten samples were forged, five of which were forged with three hammer strokes (HS) while the other five samples were forged with five HS. The forging force was 750 kg. The forging process was carried out in the State

Company for Automotive and equipment Industry (S.C.A.I.) in Alexandria, Babylon. Table (3.4) explains the experiments of the current study.

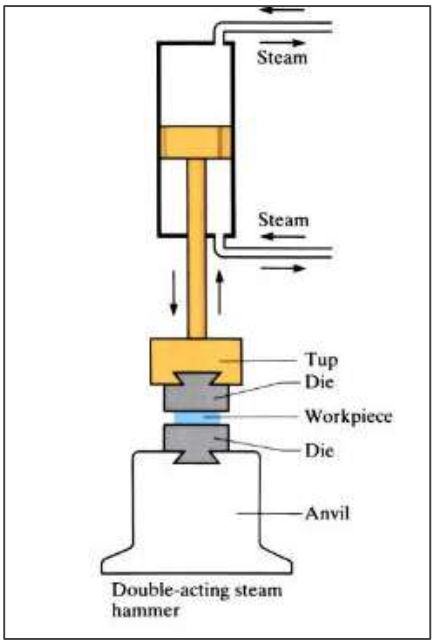

Figure (3.6): Schematic representation of open die forging process.

Table (3.4): Experiments of the current study.

Deposition Pattern	WAAM	WAAM+3 HS	WAAM+5 HS
Longitudinal	A1	B1	C1
Transverse	A2	B2	C2
Right Network	A3	B3	C3
Oblique	A4	B4	C4
Oblique Network	A5	B5	C5

3.5 Preparation of Test Specimens

Specimens were prepared for tensile, micro-hardness, microscopy (optical and SEM) and EDS tests, according to ASTM. The specimens used for the hardness and microscopy tests were cut without removing the substrate material to perform these tests across the interface between the

additive layer and the substrate, using BS-712N metal cutting saw machine. For the tensile test specimens, the substrate material was removed using the milling process before extracting the required specimens from the locations shown in Figure (3.8).

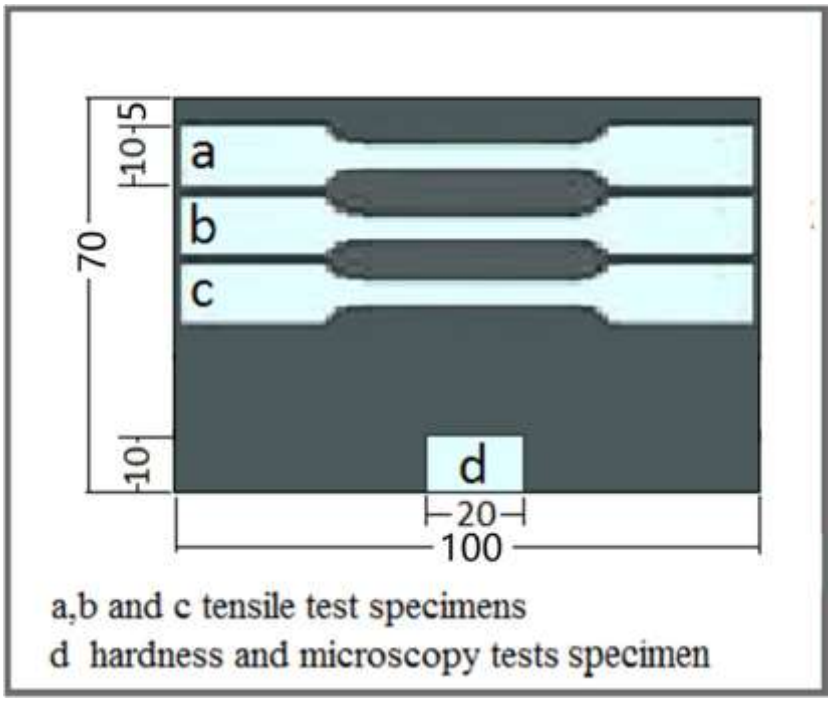

Figure (3.7): Locations and dimensions of the test specimens.

3.7 Microscopy

3.7.1 Optical Microscopic Inspection

Specimens for microstructural analysis were prepared according to the standard metallographic techniques that involve the following steps.

1- Specimens were cut to a suitable size to facilitate handling and detect the microstructural variations in different zones.

2- The wet grinding process was carried out by exposing the specimen surface to the rotary disk using emery papers of SiC with different grades

in sequence (80,220,400, 600, 800, 1000, 1200 and 1500). The specimen was then washed with water and dried with hot air.

3- Mechanical Polishing: Diamond particle pastes were used to remove the new finer scratches introduced by the grinding step. Polishing was achieved using 3, 1 and 0.25 μm pastes sequentially; the polishing was applied on special clothes fixed on electrically powered rotary discs.

4- Etching: Nital (2% HNO_3 + 98% Methanol) was used as an etchant to reveal the phases by its chemical effect on the different phases in various levels. Following the etching, the prepared surface to be examined was cleaned with alcohol.

An optical microscope was then used to determine the microstructure and topography of the different regions of the additive metal and the substrate. This test was conducted in the labs of the Department of the Metallurgical Engineering-Faculty of Materials Engineering -University of Babylon.

3.7.2 Scanning Electron Microscopy

Microstructural examination and chemical composition analysis were carried out using SEM and EDS at Al-Razi Center for Metallurgical Examinations in Tehran-Iran. SEM images were taken for all prepared specimens in order to deeply investigate the microstructure with higher magnifications. The specimens were prepared with suitable grinding papers, polished and then etched by nital solution with the same steps as in the optical microscopy. Three regions of the additive metal (upper, middle and lower regions) and the substrate metal were studied. The EDS was then performed in order to obtain the elemental analysis.

3.8 Mechanical Tests

3.8.1 Micro-hardness test

Micro-hardness test was carried out using digital Vickers micro-hardness tester type (HVS-1000) according to ASTM E384-17. Three regions of the additive metal (upper, middle and lower regions) and the substrate metal were measured after grinding the surfaces being tested. This test was done with a load of 500 g and loading time of 10-15 seconds. The measurement point distribution was by 1.0 mm intervals across the additive layer-substrate interface, with two measurements per point. This test was done at Al-Razi Center for Metallurgical Examinations in Tehran-Iran.

3.8.2 Tension test

Figure (3.9) shows the shape and dimensions of the tensile test specimen. The specimens were extracted from the additive material by wire electro discharge machining (W-EDM) cut to be as shown in Figure (3.10). The tensile strength value was an average of three. The test was carried out via universal device WAW-200 China according to (ATSM E8/E8M−13a) with a speed of 1 mm/min. at the labs of the Metallurgical Engineering Department-Faculty of Materials Engineering-University of Babylon.

G=50, W=6, T=5, L=100, A=32, B=30, C=10, R=6 (mm).

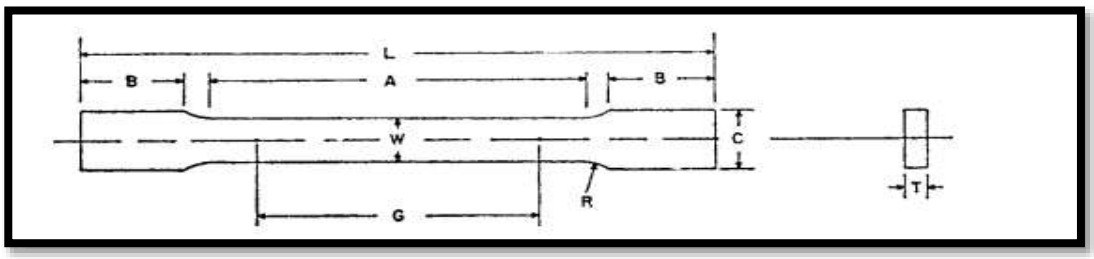

Figure (3.8): Shape and dimensions of the tensile test specimen.

3.9 Fractography Observation

This test was performed on tensile specimens after fracture. The aim of this test is to determine the type, size and location of possible defects which can be easily seen by the naked eye as photographed, in addition to identify the fracture mode.

CHAPTER FOUR:

RESULTS & DISCUSSION

RESULTS AND DISCUSSION

4.1 Introduction

This chapter explains and discusses the results obtained from the experimental work. Microstructural analysis of the WAAM samples will be performed using the OM and SEM with the help of the EDS. The results of mechanical tests for the samples, such as Vickers micro-hardness and tensile strength, will also be discussed.

4.2 Micrography

4.2.1 Unaffected Substrate Material

Before evaluating the microscopic variations in the WAAM samples, it is necessary to understand the structure of the substrate material manufactured from the AISI 5155 low alloy steel with the chemical composition shown in Table (3.3). Figure (4.1) exhibits that the microstructure of the substrate material contains mostly pearlite, composed of sequential lamellar layers of ferrite and cementite, with a low-volume fraction of ferrite.This is the normal structure for an alloy that has such a composition in the annealed state.

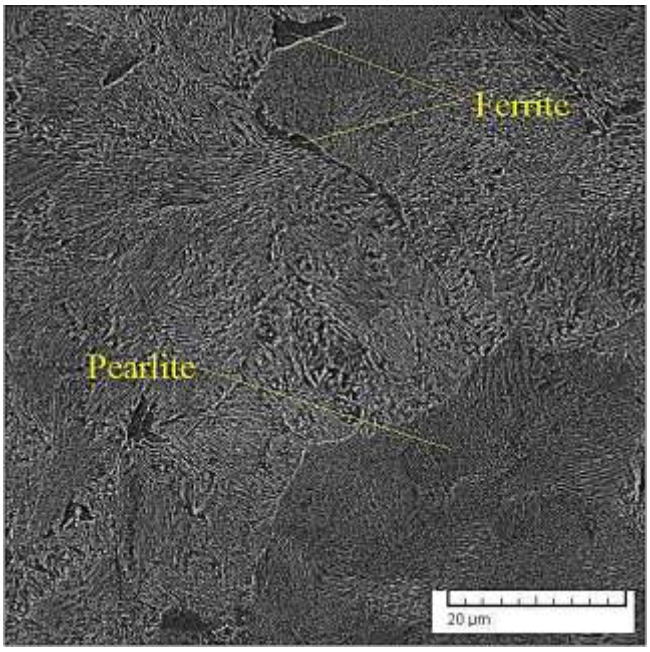

Figure (4.1): Microstructure of the substrate material using SEM.

4.2.2 Wire Arc Additive Manufacturing Samples

Microscopy along the cross-section of the additive material deposited longitudinally (A1 in Table 3.6) shows in Figure (4.2) a diversity of microstructure in different regions (upper, middle and lower regions). The dominant structure of the additive material contained, as primary micro-constituents, ferrite and a lower-volume fraction of lamellar pearlite. This is in agreement with that obtained by Ron et al. (2019) **[80]**. The lower region of the additive built material showed a relatively coarse equiaxed grains. It is supposed that the metal grains of the first deposited layers were large columnar as a result of the higher cooling rates to which these layers are exposed due to the rapid absorption of heat by the cold substrate plate. These columnar crystals have been recrystallized to relatively coarse equiaxed grains by the heat of the deposited middle metallic layers. The middle region showed a relatively finer equiaxed grains. It is assumed that the columnar grains of the metal deposited in this region were finer as a result of the lower cooling rates due to the effect of preheating by the previous deposited layers **[80]**. These columnar grains will then be recrystallized to finer equiaxed grains by the heat of the deposited upper layers. The upper region however exhibited columnar grains because there were no subsequent layers to recrystallize; this is in agreement with that obtained by Aldalur et al. (2020)**[85]**.

The pearlite content in the lower region of the additive built material was more than that in the middle region, which in turn was more than that in the upper region. This is due to the dilution effect with the substrate material **[82]**, which appears more clearly in the built layer/substrate interface region (Figure 4.3). For the middle and upper regions, the proportion of pearlite was lower, since the carbon content in the filler wire raw material is relatively low (0.08%) **[82]**.

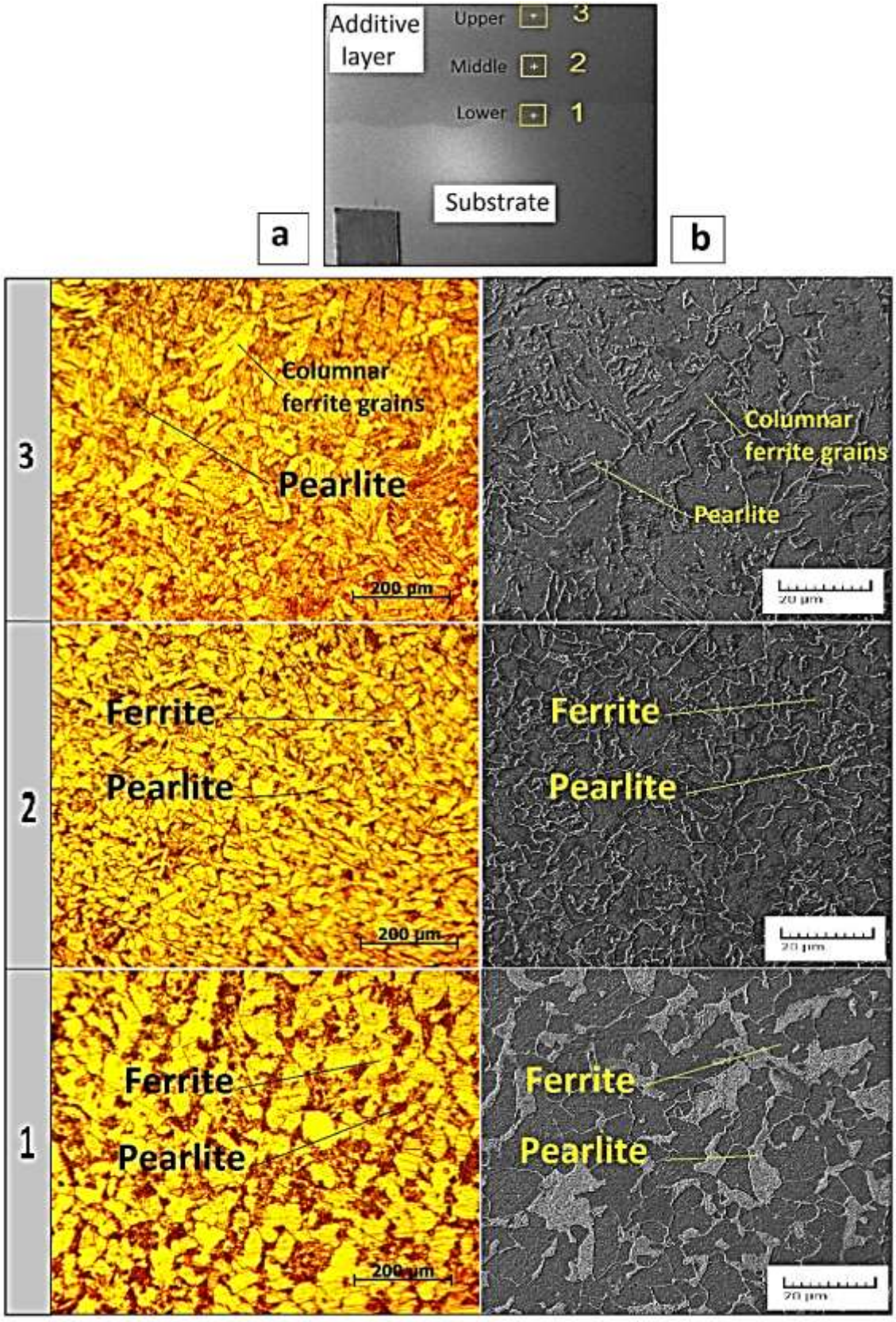

Figure (4.2): Micrography of the different regions along the cross-section of the A1 sample using (a): OM and (b): SEM.

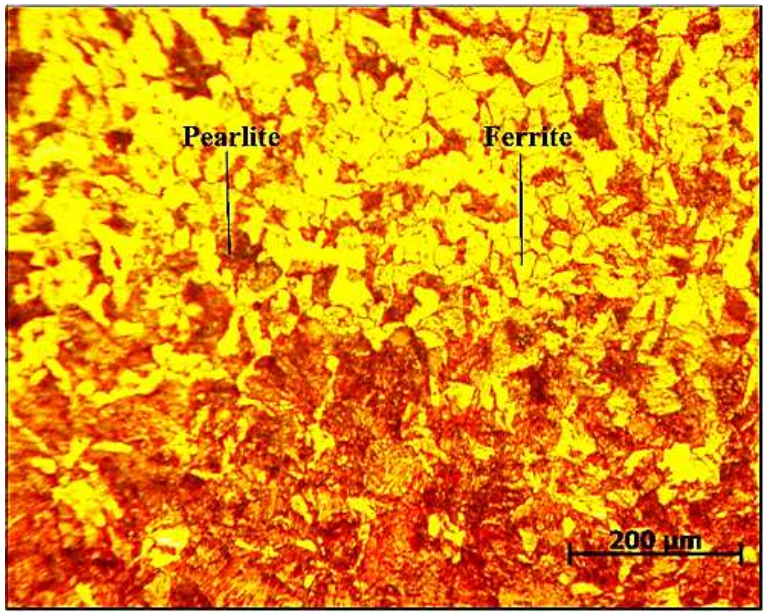

Figure (4.3): Microstructure of the built layer/substrate interface region of A1 sample.

Microstructural examination along the cross-section of the additive material deposited transversely (A2) shows in Figure (4.4) a diversity of microstructure in different regions. As for the A1, the microstructure of the A2 additive metal consisted of ferrite and pearlite. Shape and size of the grains in the different regions of this sample were similar to that appeared in the A1, except for those of the upper region. The grains in this region were somewhat coarser, and the columnar grains were less compared to those appeared in the upper region of the A1 sample. This could be attributed to the fact that the AM runs required to built layers in A2 sample were more, resulting in accumulation of heat, and thus lower cooling rates **[84]**. Pearlite distribution was also similar to that in the A1 sample.

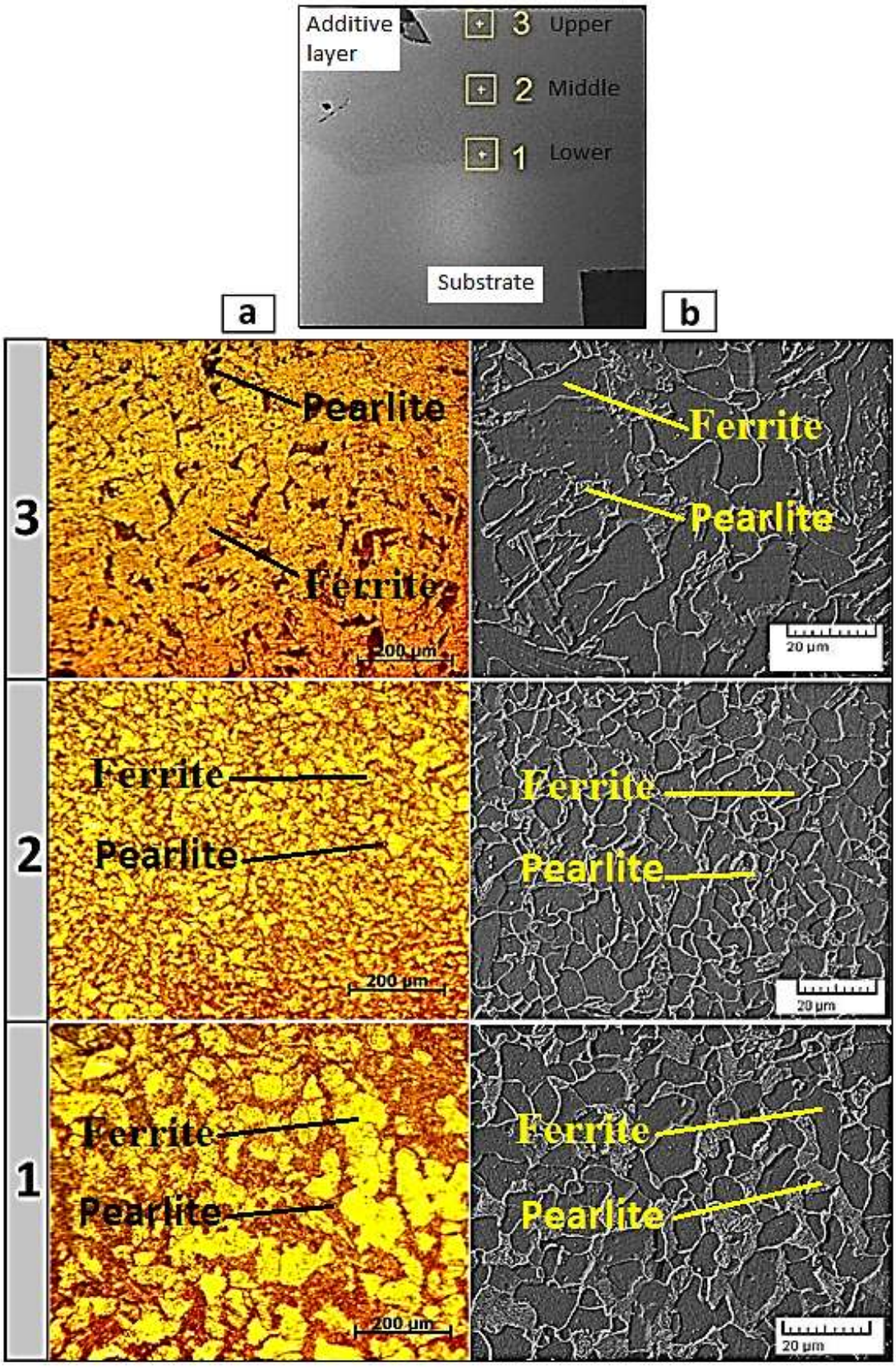

Figure (4.4): Micrography of the different regions along the cross-section of the A2 sample using (a): OM and (b): SEM.

For the A3 sample, the microscopy of the lower region showed in Figure (4.5) a microstructure finer than that appeared in A1 and A2 samples; this is in line with that obtained by Aldalur et al. (2020)**[85]**. This may be due to that the first layer was built longitudinally before depositing the second layer transversely. Therefore, the more runs as a result of the transverse deposition led to the heat accumulation, and thus more recrystallization.

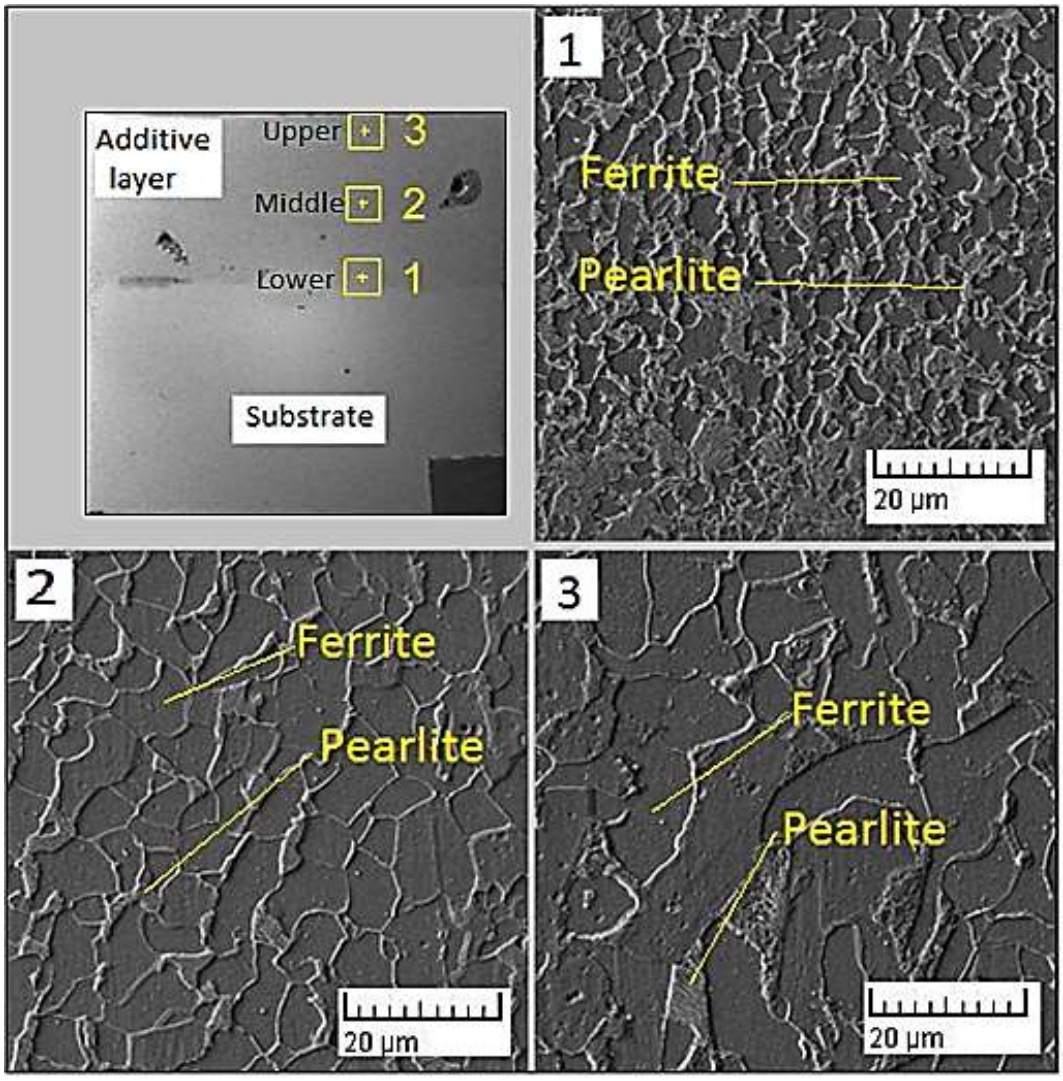

Figure: (4.5) Microscopy for A3 sample in the different regions using SEM.

Micrography in Figure (4.6) for the A4 sample showed that the shape and size of the grains in the different regions of this sample were similar to that appeared in the A3, except for those at the lower region. Clearly, the grains in this region were coarser. However, microstructural examination for the A5 sample were somewhat similar to that appeared in the A4 as shown in

Figure (4.7).

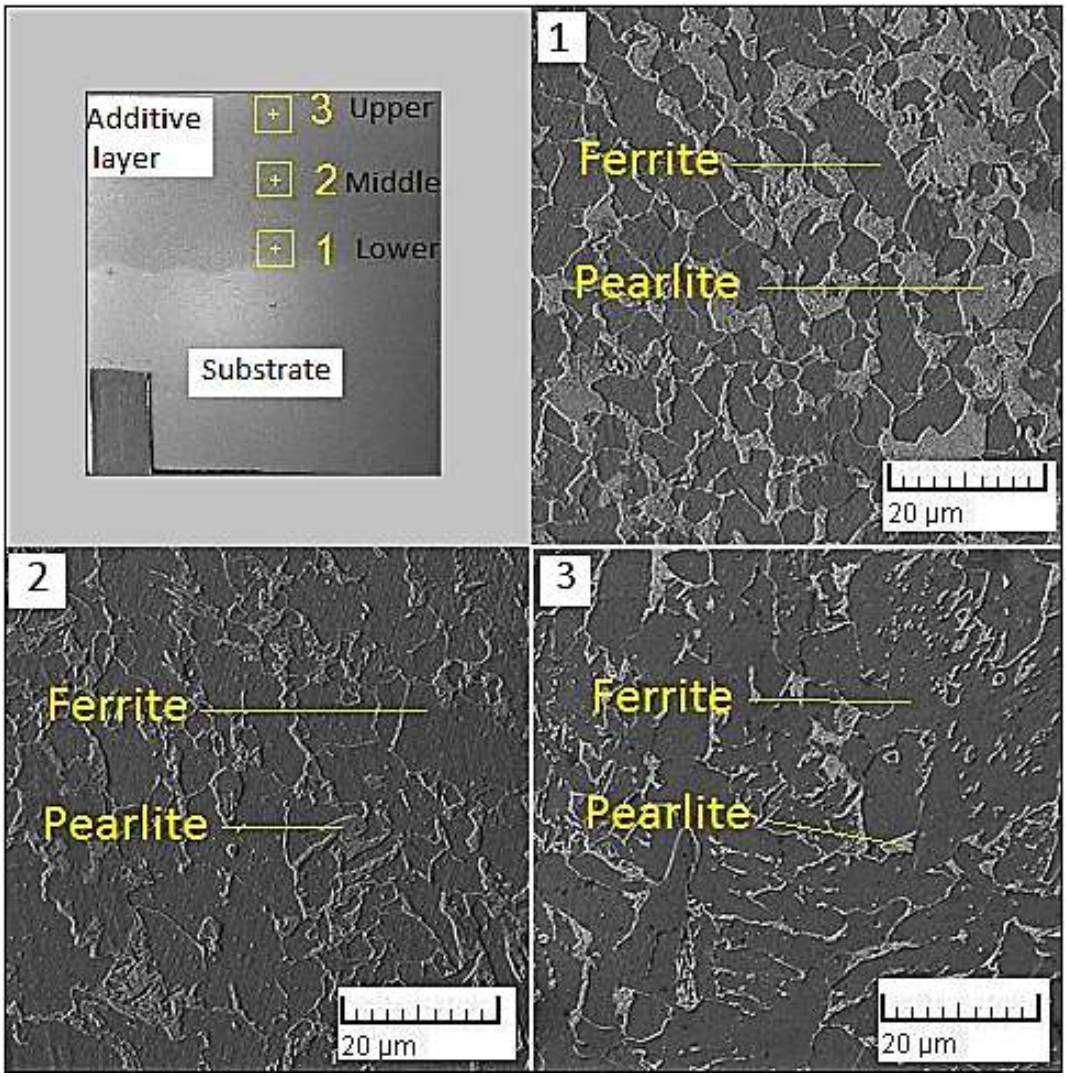

Figure (4.6): Micrography for the A4 sample in the different regions using SEM.

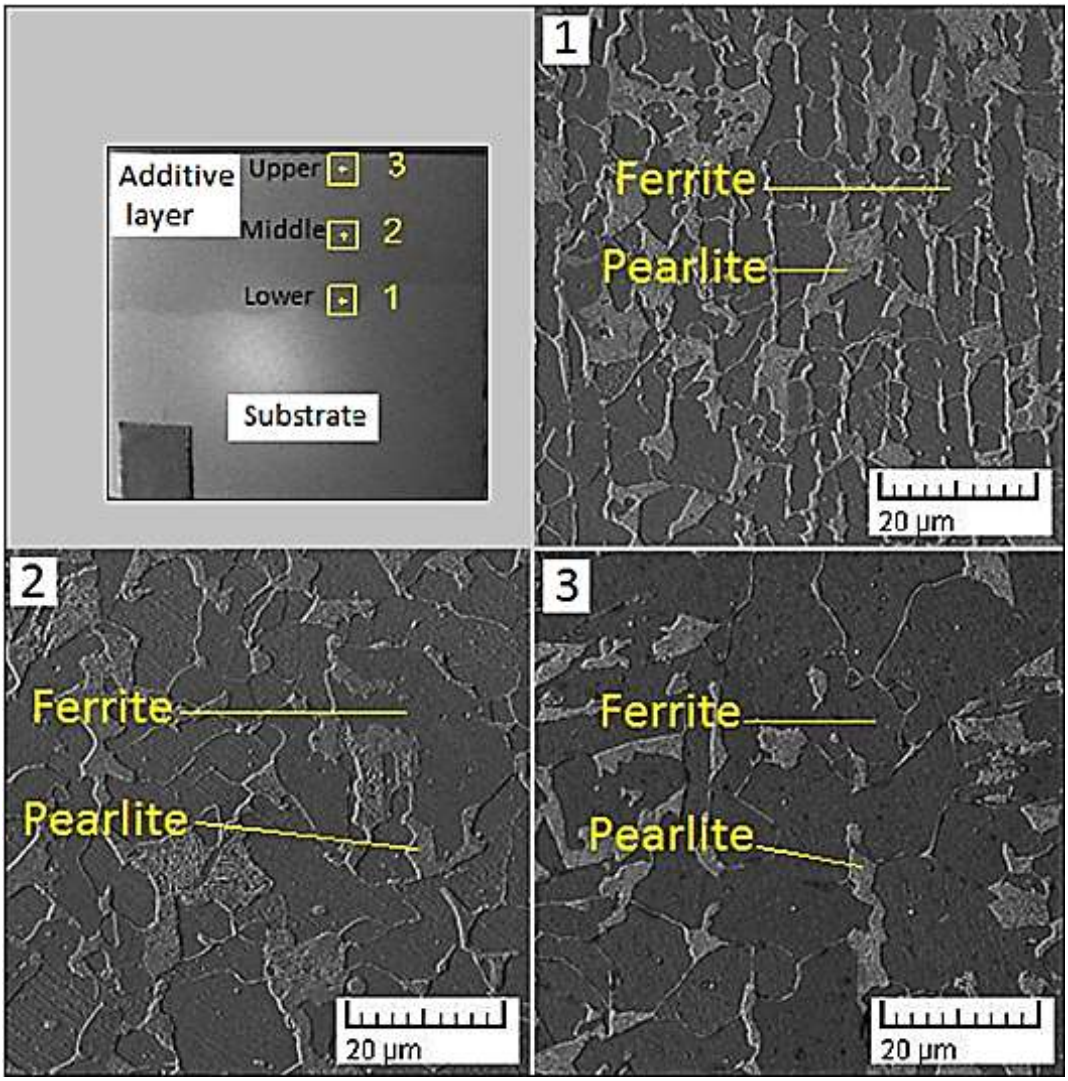

Figure (4.7): Microstructure of the A5 sample in the different regions using SEM.

4.2.3 Influence of Cold Forging Process on the Microstructure of Wire Arc Additive Manufacturing Samples

Cold forging for samples built with different deposition patterns using a forging force of 750 kg with three HS (B Samples) and five HS (C Samples) resulted in rather noticeable changes, especially at the upper layers of the deposited material. Effect the forging by five HS was however more. Figure (4.8) explains microstructures of samples built with two different deposition patterns after forging with five HS. The figure predominantly shows elongated grains as a result of the effect of the forging process.

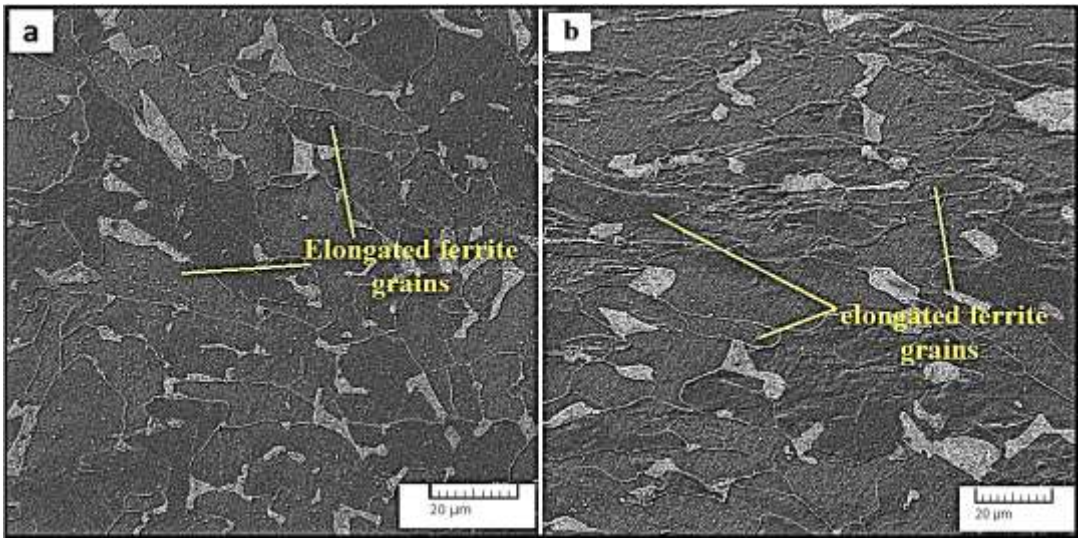

Figure (4.8): Microstructure at the upper layers of (a): C1 sample (b): C4 sample.

4.3 Energy Dispersive Spectrometer (EDS)

Figure (4.9) shows the EDS examination of A1 sample at the layer/substrate interface region.

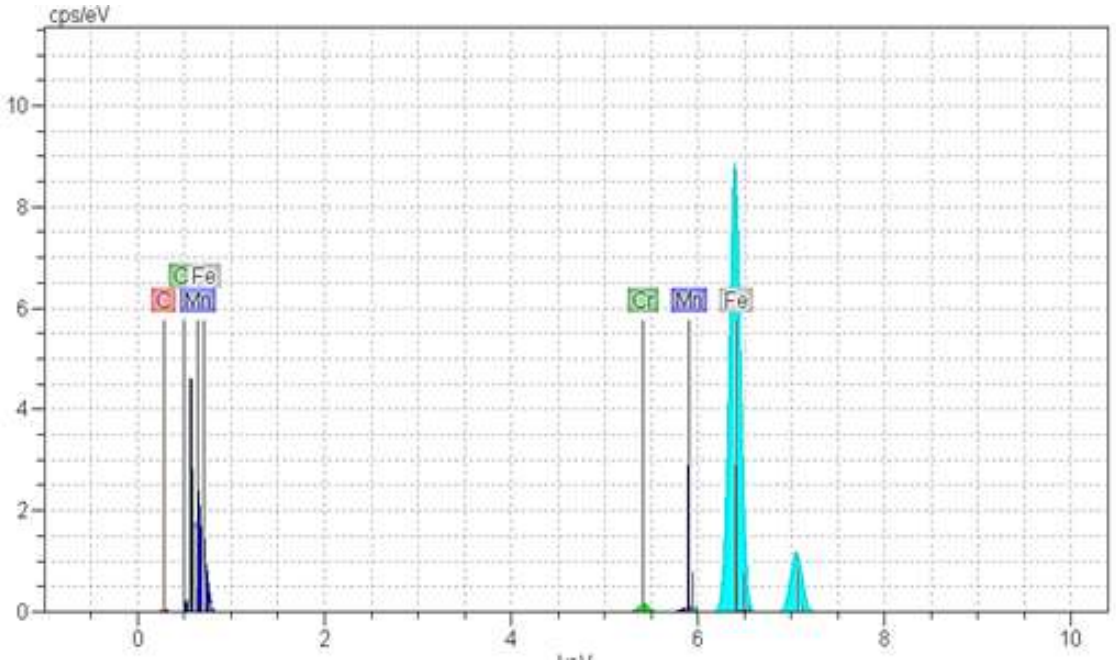

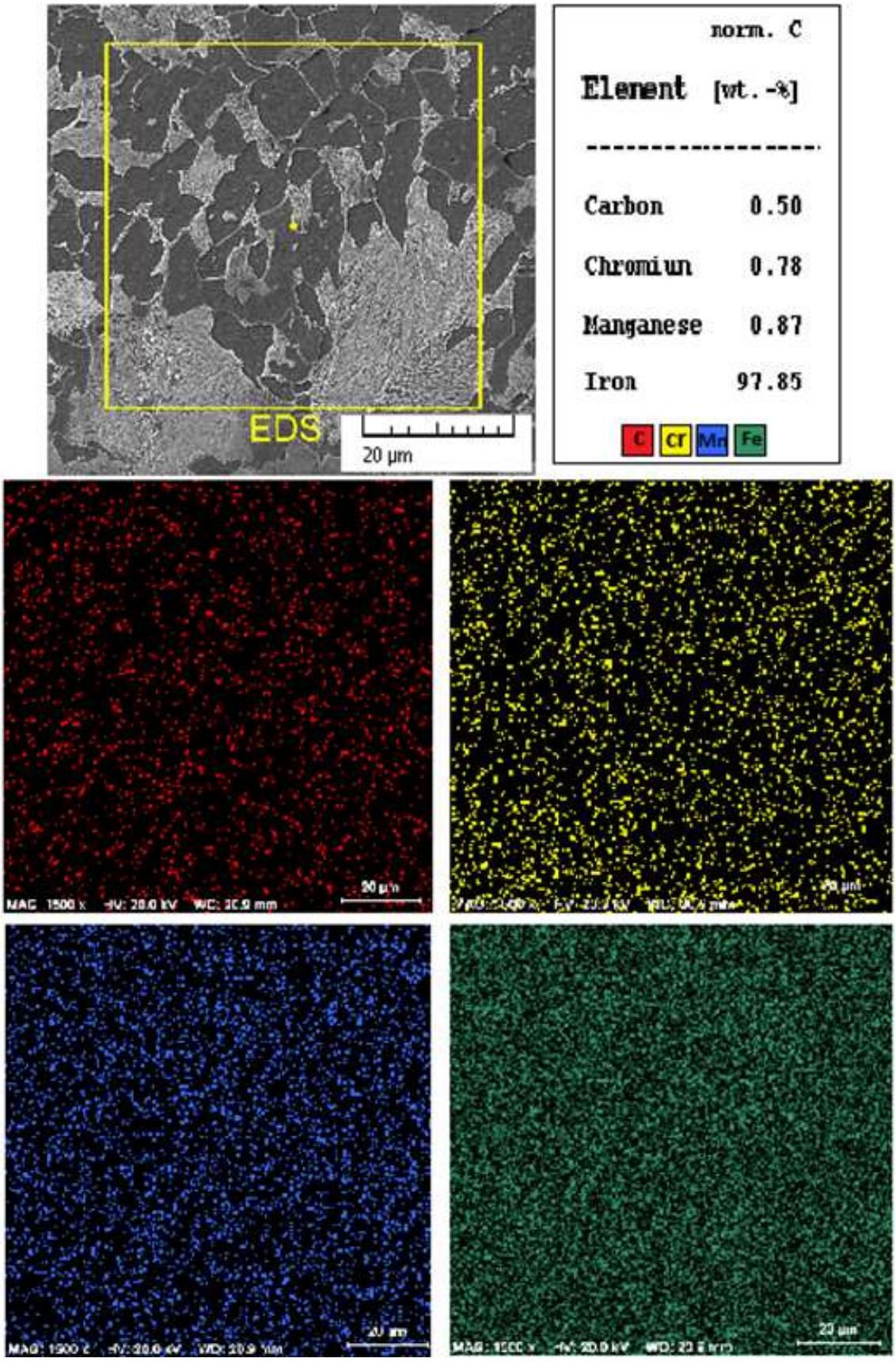

Figure (4.9): EDS examination of A1 sample

The proportions of chromium (Cr), manganese (Mn) and iron (Fe) were 0.78, 0.87 and 97.85% respectively. The proportion of Cr was almost similar to that of the substrate material, because there is no Cr in the filler wire raw material (Table 3.4). Mn proportion was however slightly more than that of the substrate material (Table 3.3), due to the relatively high proportion of Mn in the filler wire material (1.5%).

The chemical composition analysis of samples A2, A3, A4 and A5 at the layer/substrate interface region exhibits in Figure (4.10) different proportions of Cr, which are close to some extent to those present in the substrate material, due to the absence of Cr in the filler metal. Some samples showed a higher proportion of Mn. This might be due to the high proportion of Mn in filler wire material.

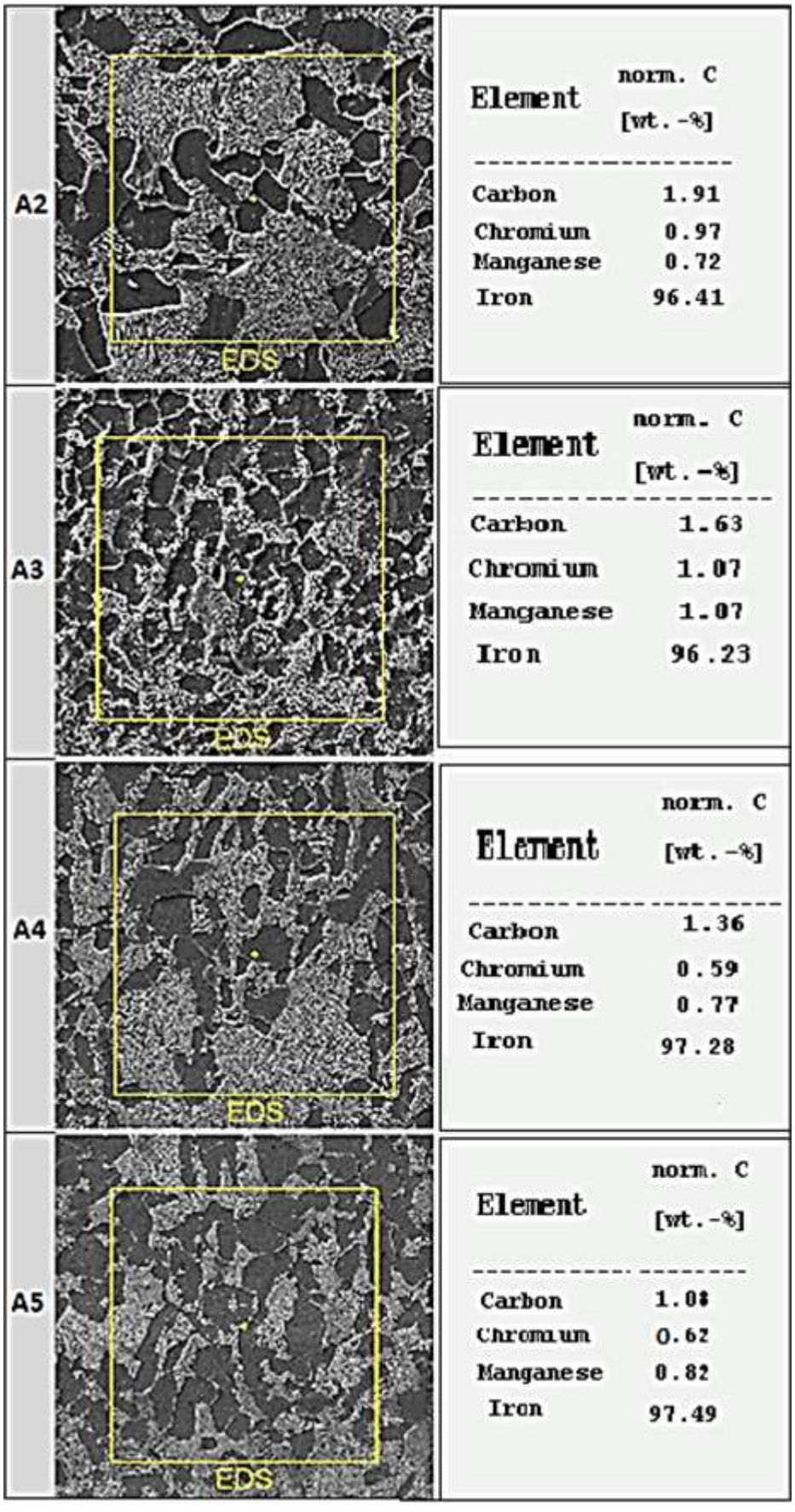

Figure (4.10): Chemical composition analysis of samples A2, A3, A4 and A5.

4.4 Micro-hardness Test

A number of microstructural changes caused the expected variance in hardness across the additive layers. The simplest method for evaluating the additive layers quality, and consequently the performance of the additive layers, is the hardness test. It is also important as a way to differentiate the different additive layers. The hardness value of the substrate material was the highest (265HV) because the microstructure of the substrate material was mostly pearlite, and the lowest was at the additive material due to the predominant soft ferrite phase. The average value of hardness was however at the built layer/substrate interface region.

4.4.1 Wire Arc Additive Manufacturing Samples

Vickers micro-hardness test along the cross-section of the additive material deposited longitudinally (A1 sample) showed in Figure (4.11) a diversity of hardness at the different regions (upper, middle and lower regions). Hardness at the lower region was higher, although the equiaxed grains in that region were coarser. This can be attributed to the fact that the fraction of pearlite in that region was higher. The middle region showed less hardness than that at the lower region, because the percentage of pearlite was significantly lower, although the structure of this region was of smaller grain size. The upper region showed less hardness than those at the other regions, for two reasons: the first is that the fraction of pearlite in this region was the lowest, and the second reason is that the particle size in this region was coarser (columnar grains). It is known that the pearlite structure exhibits higher hardness than ferrite due to the presence of the hard cementite phase within the lamellar pearlite structure **[86]**. It is also known that reducing the particle size leads to an increase in hardness and strength, due to the increase in the amount of grain boundaries, which have higher hardness and strength at room temperature than grains **[91]**; act as barriers to hinder the dislocations **[92]**.

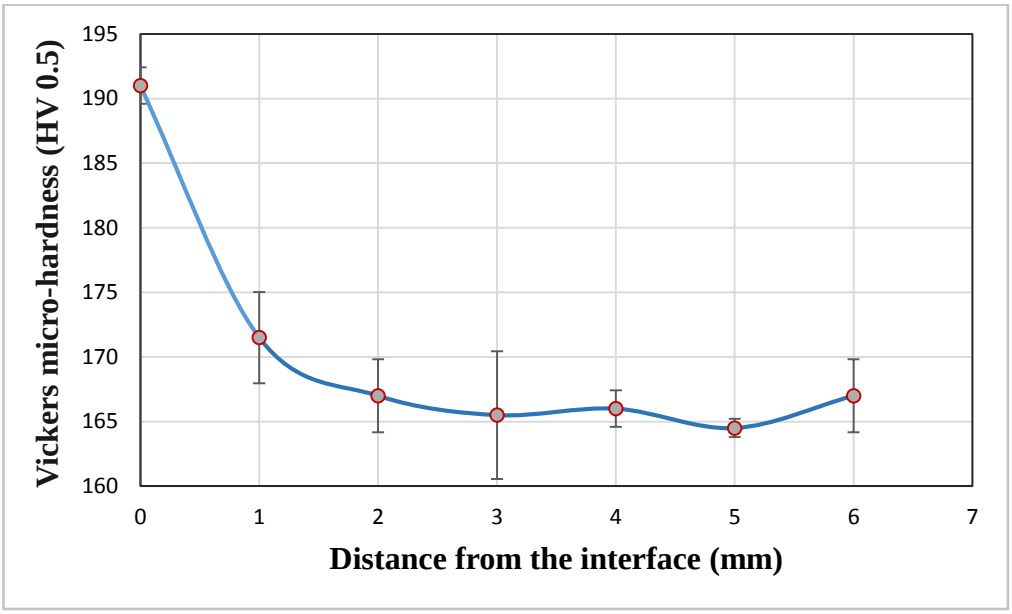

Figure (4.11): Hardness distribution across the different regions of A1 sample.

The hardness value at the built layer/substrate interface region was (191HV), which is significantly higher than that of the additive layer material (Figure 4.11), which in turn is less than that of the substrate material (265HV). This is because the pearlite content in the built layer/substrate interface region was an average between the pearlite content of the substrate and the additive material.

The hardness distribution along the cross-section of the additive material deposited transversely (A2 sample) was similar to that in A1 except for the significant decrease in the hardness values at the upper layers of the sample. This is because the microstructure at that region was somewhat coarse.

The microstructure of the lower region in sample A3 was finer than that in A1 (Figure 4.5), so the hardness values in that region were somewhat higher, while the rest of the hardness distribution along the cross-section of the A3 sample was similar to A1. Although the structure of the lower region of the sample A4 was coarser than that of A3, hardness at that region was higher. This may be due to the content of pearlite in the region for which the test has been conducted, especially the distribution of pearlite in that region, close to the interface, was not homogeneous.

The hardness distribution along the cross-section of sample A5 was however similar to that of the other samples, with the hardness being highest at the lower region adjacent to the interface, and gradually decreased while advancing towards the upper region. This is due to the effect of the pearlite content as a result of the dilution and the size and shape of the resulting grains.

4.4.2 Influence the Cold Forging Process on Hardness of Wire Arc Additive Manufacturing Samples

Figure (4.12) shows the average hardness of the AM samples deposited with different patterns without forging, and with cold forging by (3 HS and 5 HS). It is evident from the figure, in general, a significant increase in the average hardness of the built materials for the samples deposited with different patterns and forged, compared with their non-forged counterparts. Hardness of the samples forged by (5) HS was higher than that forged by (3) HS. This is due to the effect of the cold forging process on the resulting microstructure, especially in the upper regions of the deposited material, where the elongated grains (Figure 4.8) as a result of the forging process lead to an increase in hardness **[93]**.

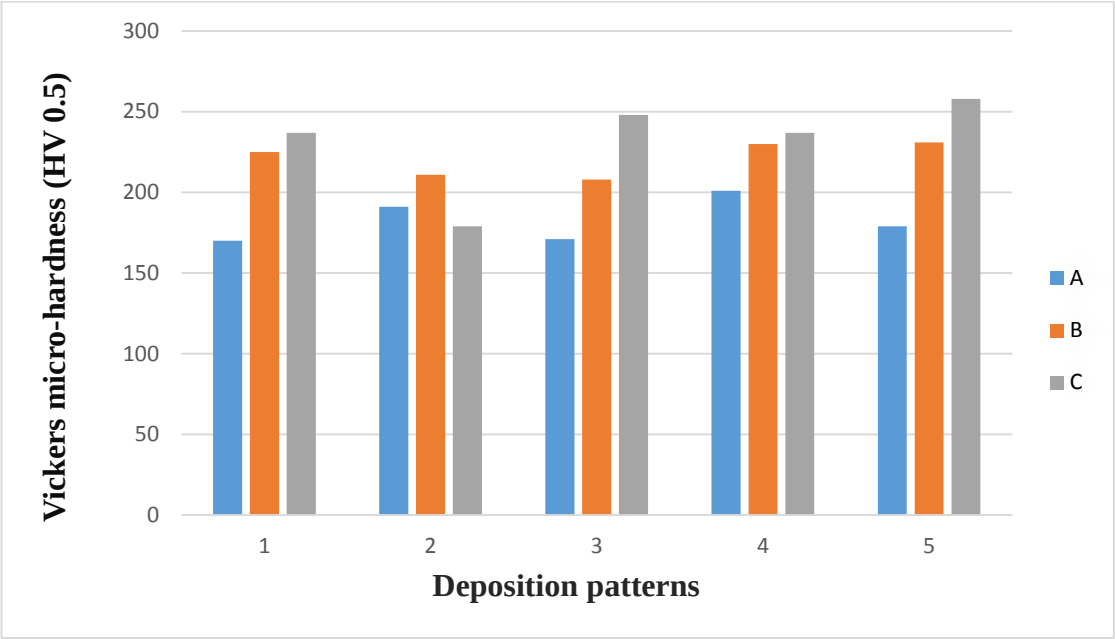

Figure (4.12): The average hardness of the AM samples deposited with different patterns (a): without forging, and with cold forging by (b): 3 HS and (c): 5 HS.

4.5 Tensile Test

4.5.1 Wire Arc Additive Manufacturing Samples

One of the most important goals of this study is to determine the tensile strength of the deposited AM material. Tensile test specimens were extracted from different samples; these specimens include all the deposited layers (upper, middle and lower). The average tensile strength value of the additive material deposited longitudinally (A1 sample) was somewhat high (480 MPa) as shown in Figure (4.13). This is due to the fact that the direction of tension during the tensile test was parallel to the direction of deposition of the additive layers. The microstructure resulting from the deposition of the metal using this pattern was mostly equiaxed grains with various grain sizes according to the locations of the deposited layers. For the same reason, the fracture was significantly ductile (Figure 4.14), and the load-deformation curve shown in Figure (4.15) proves this, as it is evident from the figure that the elongation was notably large.

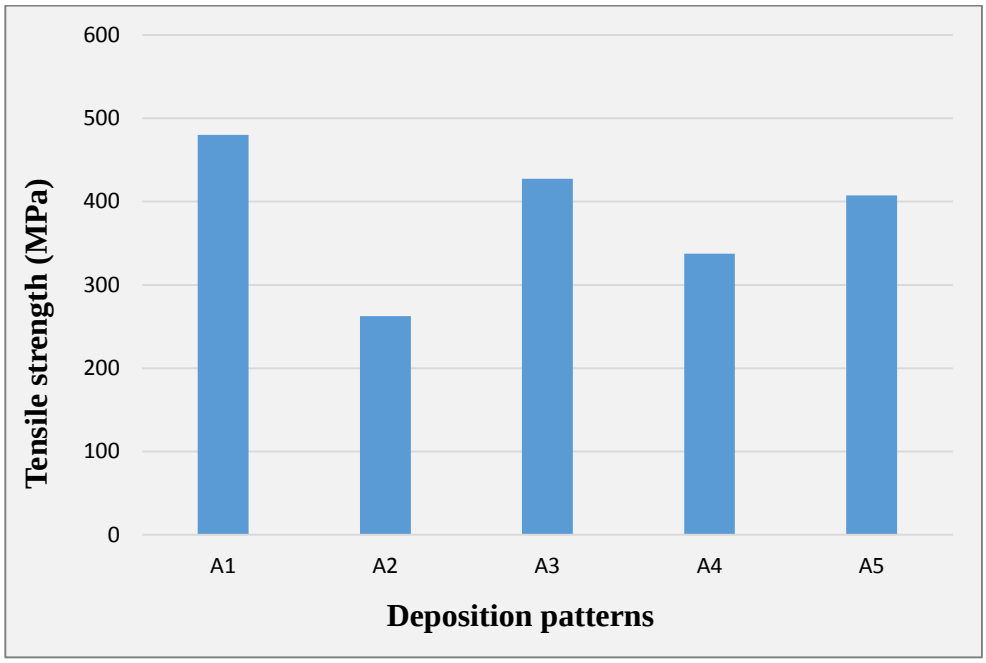

Figure (4.13): The average tensile strength of the AM material deposited with the different patterns.

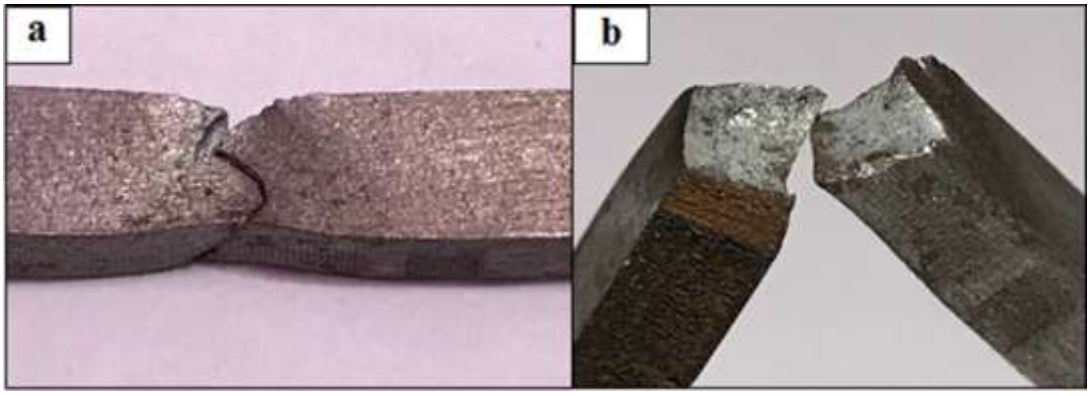

Figure (4.14): Fracture of one of the A1 tensile test specimens (a): fracture mode (b): cross-section of fracture.

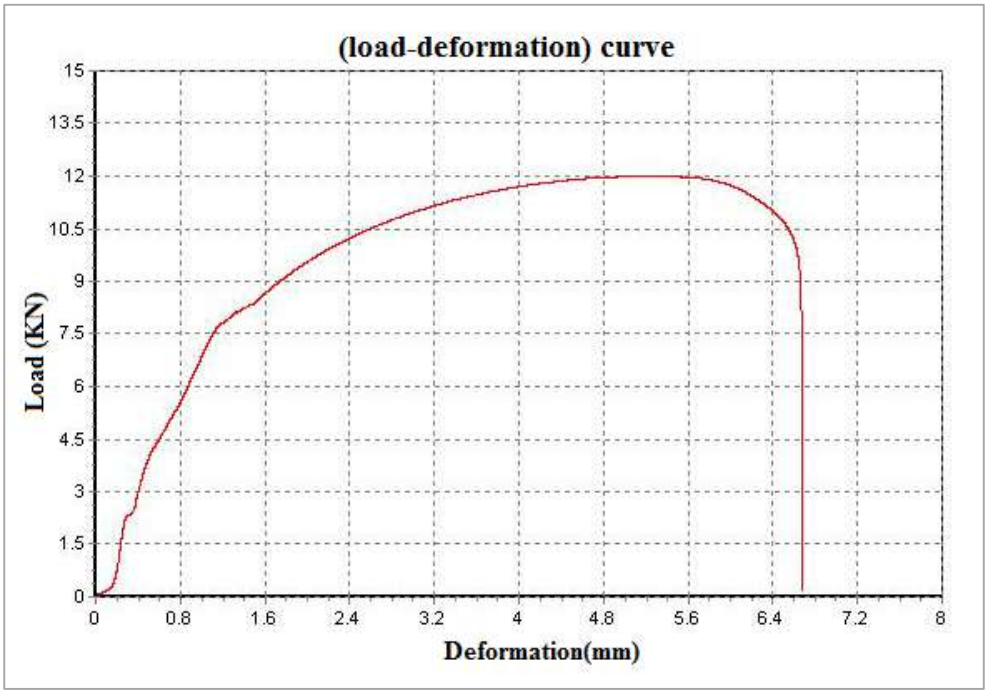

Figure (4.15): Load-deformation curve of one of the A1 tensile test specimens.

Figure (4.13) shows that the average tensile strength value of the deposited AM material of the A2 sample was (262.5 MPa) significantly lower than that of A1, as it is close to (55%) of the tensile strength of the specimens extracted from the A1 sample. This is consistent with what was obtained by Waqas et al. (2019). The reason for this relatively low value is that the tension direction was perpendicular to the deposition direction of the additive layers, with a possibility of fracture occurring from convergence regions of the deposition runs for each layer. Figure (4.16) shows that the fracture was not ductile as in the A1 sample, but rather brittle. This is also evidenced by the load-deformation curve of this sample, which is shown in Figure (4.17), where the elongation was much lower.

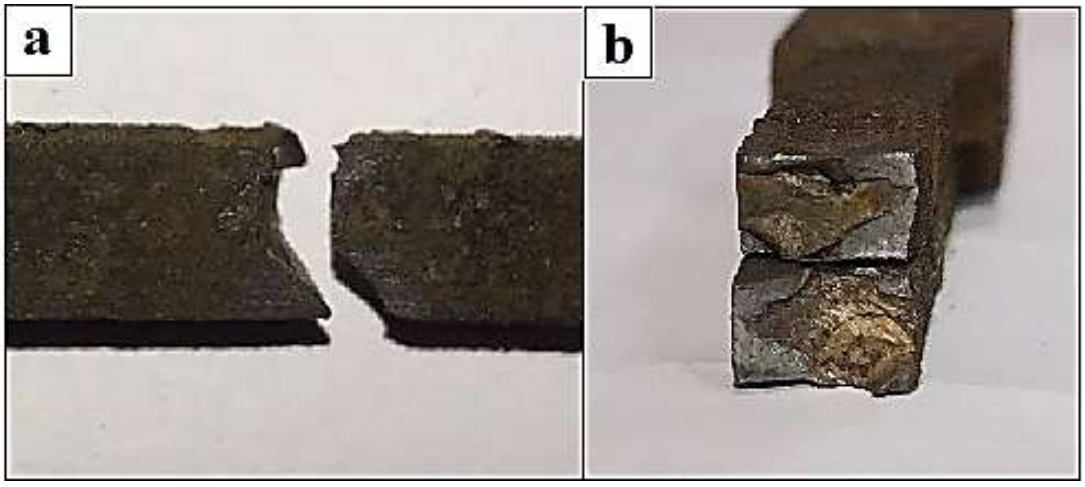

Figure (4.16): Fracture of one of the A2 tensile test specimens (a): fracture mode (b): cross-section of fracture.

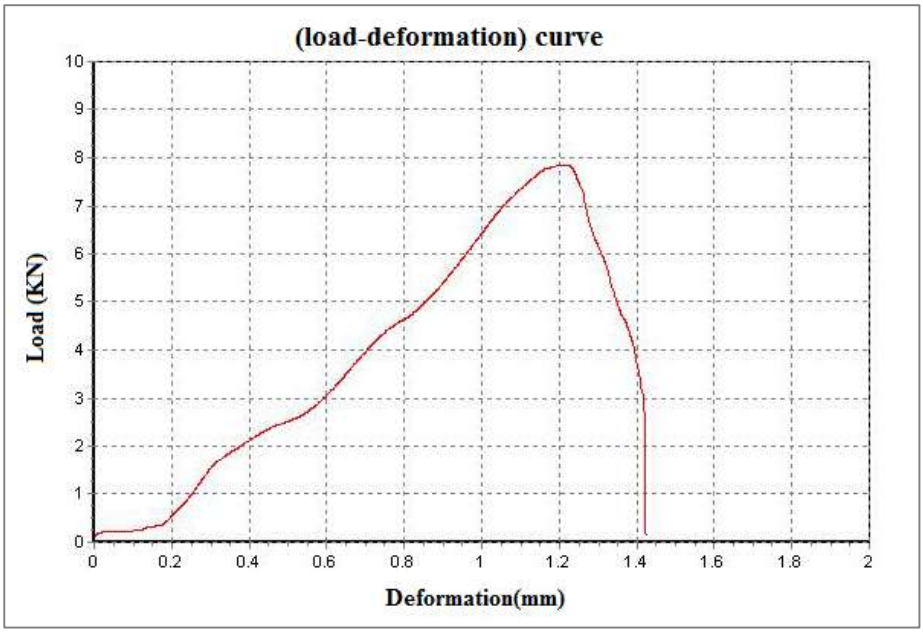

Figure (4.17): Load-deformation curve of one of the A2 tensile test specimens.

The average tensile strength value of the specimens extracted from A3 sample was (427.5 MPa), which is about 1.6 times (significantly higher than) that of the A2 sample. This is due to the fact that the deposition of the additive layers was a right network, that is, a network of longitudinal and transverse layers. For the effect of the transversely deposited layers in this pattern, A3 sample had lower tensile strength (about 89%) than that of A1. The fracture was somewhat ductile (Figure 4.18), and the elongation was higher than that of the A2 sample as in Figure (4.19).

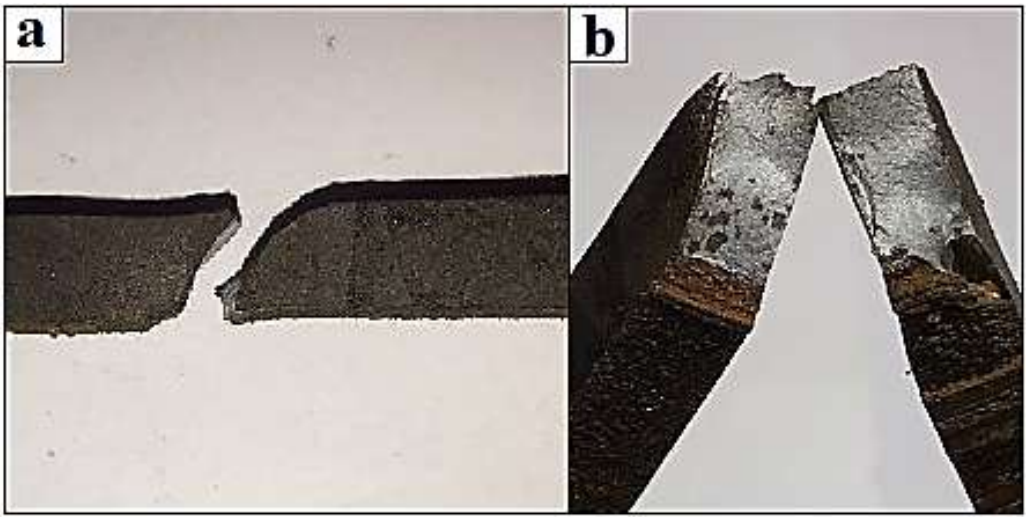

Figure (4.18): Fracture of one of the A3 tensile test specimens (a): fracture mode (b): cross-section of fracture.

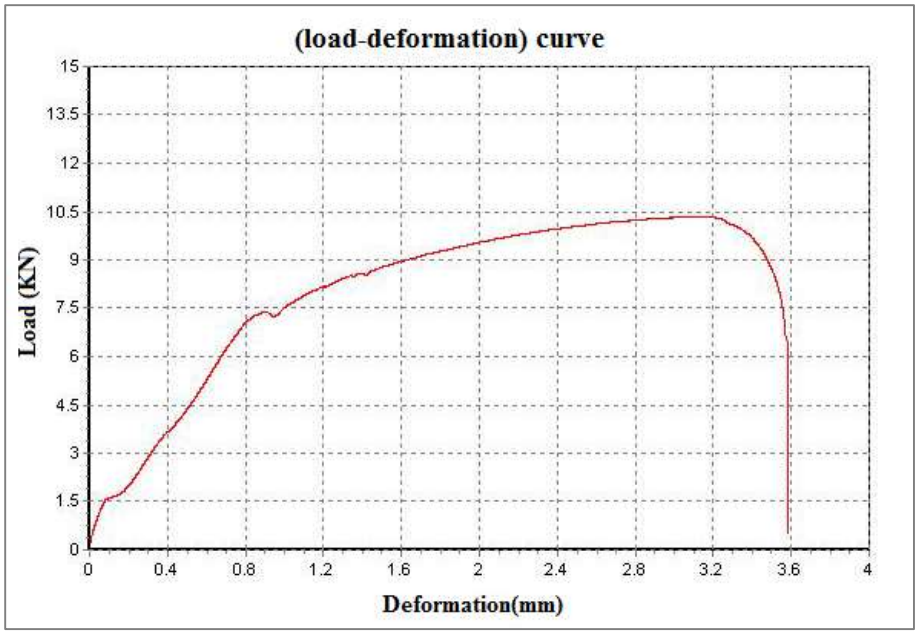

Figure (4.19): Load-deformation curve of one of the A3 tensile test specimens.

It is clearly noted from Figure (4.13) that the average value of tensile strength for the specimens extracted from A4 sample was (337.5 MPa), which is about an average value between the tensile strength of A1 and A2. This may be due to the analysis of the tensile loading applied during the test into forces parallel to the deposition direction (longitudinal) and perpendicular to the

deposition direction (transverse). Figure (4.21) shows that the fracture was ductile shear at an angle of almost 45° with the direction of the applied load, approximately indicating the deposition angle of the runs of the additive material layers (oblique pattern). This clearly refers to that the fracture occurred along the convergence regions of the deposition runs for each layer. The load-deformation curve shown in Figure (4.22) indicates that the elongation of A4 sample was notably less than that of A3.

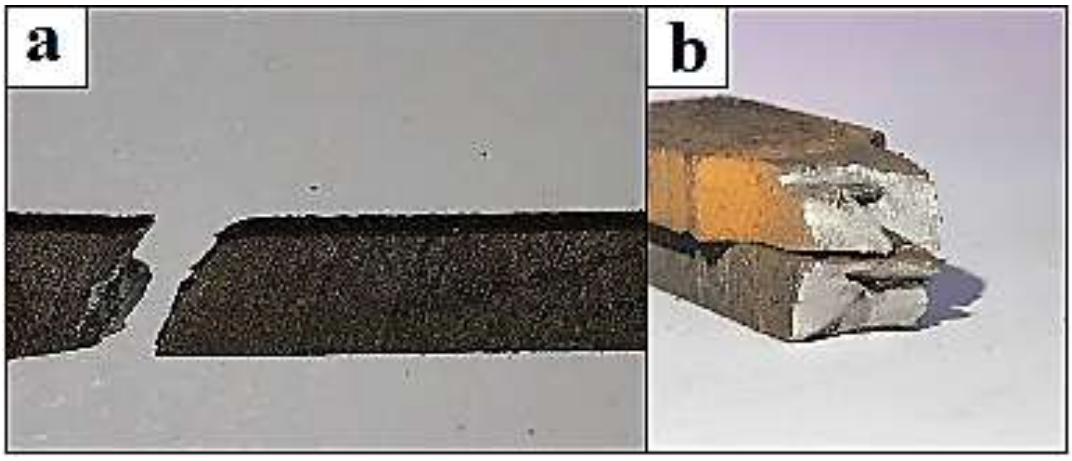

Figure (4.20): Fracture of one of the A4 tensile test specimens (a): fracture mode (b): cross-section of fracture.

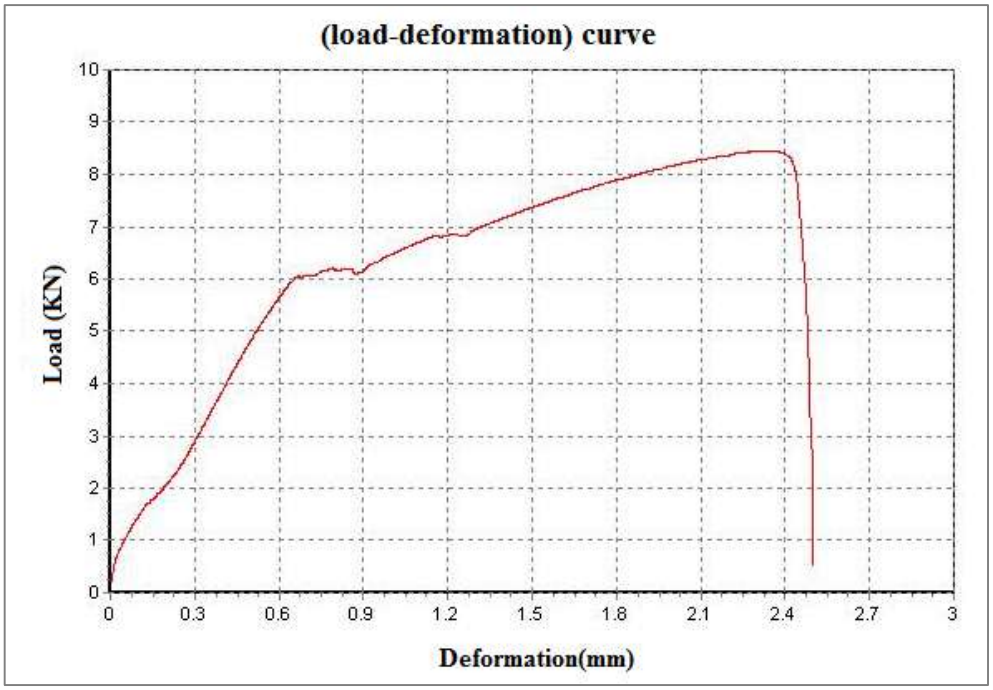

Figure (4.21): Load-deformation curve of one of the A4 tensile test specimens.

The average tensile strength value of the specimens extracted from A5 sample was higher than that of A4 (407.5 MPa) as shown in Figure (4.13). This is definitely a consequence of reducing the shear effect, because the deposition of this pattern was in the form of an oblique network. The fracture was also ductile (Figure 4.22), and the elongation was remarkably higher, as shown in the load-deformation curve (Figure 4.23).

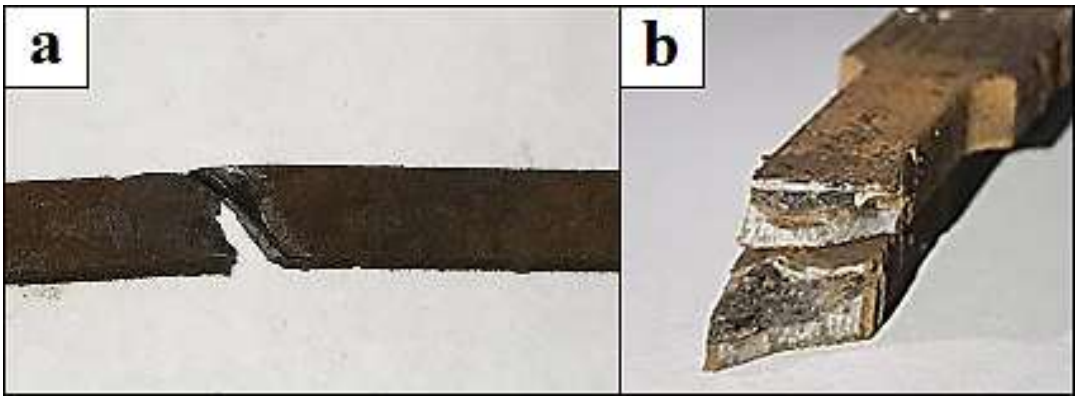

Figure (4.22): Fracture of one of the A5 tensile test specimens (a): fracture mode (b): cross-section of fracture.

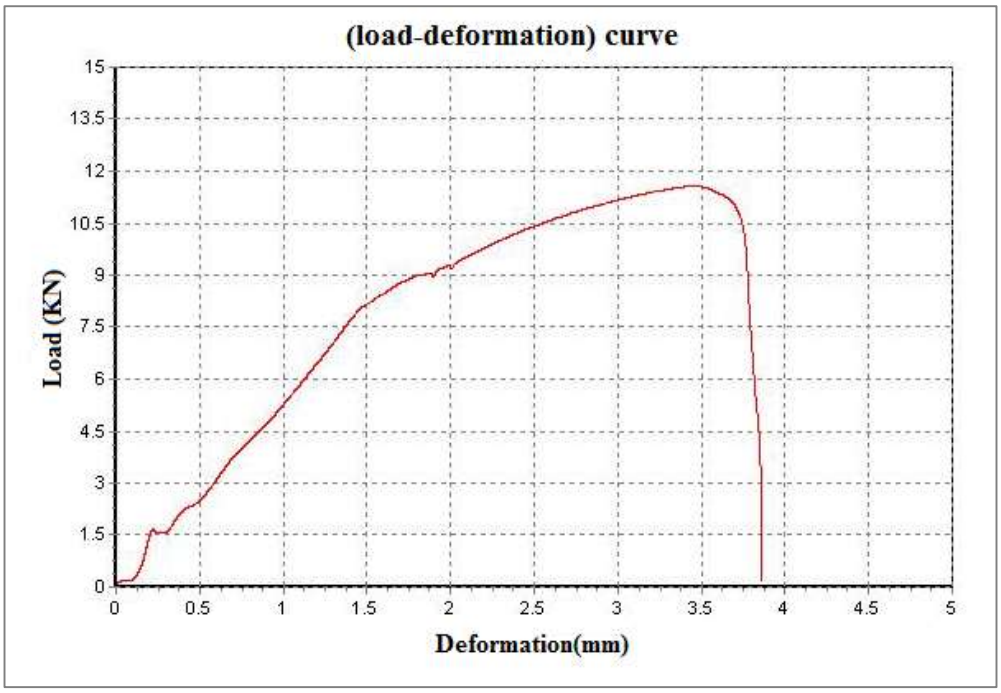

Figure (4.23): Load-deformation curve of one of the A5 tensile test specimens.

4.5.2 Influence of Cold Forging Process on Tensile Strength of WAAM Samples

Figure (4.24) illustrates the average tensile strength of the WAAM samples with and without cold forging process. It is clearly noted that cold forging introduced, in general, a noticeable increase in the tensile strength of the specimens extracted from the different samples. The average tensile strength values for the samples forged by 3 HS (B Samples) were generally slightly higher than those forged by 5 HS (C Samples). Therefore, the B samples have provided optimal tensile strength results. The reason behind the noticeable increase in tensile strength of the forged samples could be attributed to the fact that cold working in the additive layers as a result of cold forging plastically deformed the layers, and the accumulation of dislocations resulted in obstacle the dislocations growth **[94]**. Increasing hammer strikes to five strokes may result in micro-fissures between the runs of layers or between the deposited additive layers which were not detected on microscopy, thus slightly reducing the tensile strength.

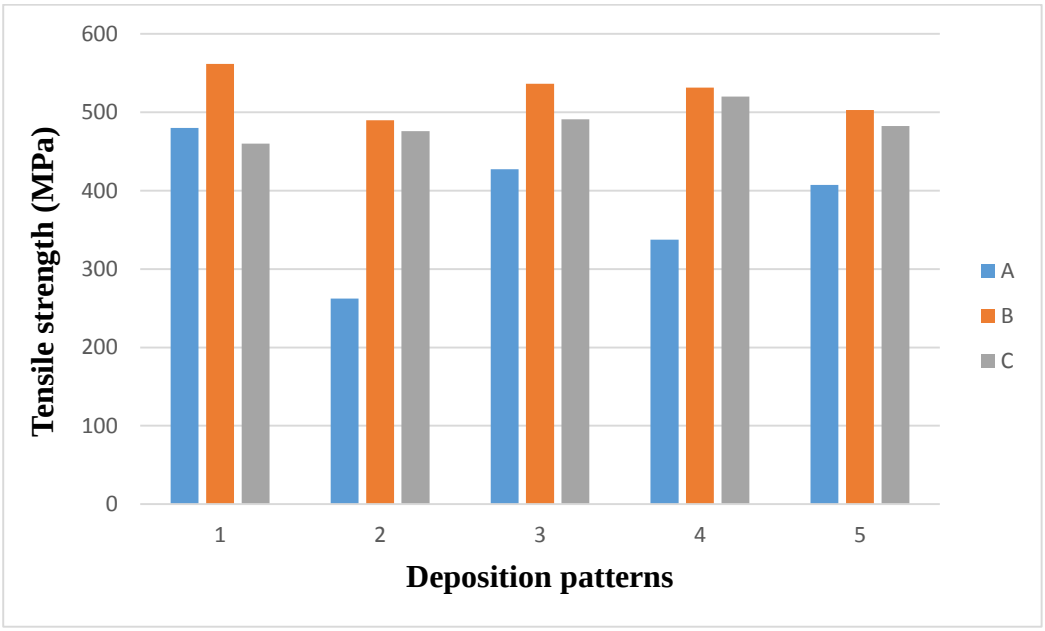

Figure (4.24): The average tensile strength of WAAM samples deposited with different patterns (a): without forging, and with cold forging by (b): 3 HS and (c): 5 HS.

CHAPTER FIVE:

CONCLUSIONS & RECOMMENDATIONS

CONCLUSIONS AND RECOMMENDATIONS

5.1 Introduction

A comparative study was conducted to analyse (15) samples of the ER70S-6 low alloy steel prepared by WAAM, using different patterns, without forging, and with cold forging by (3 HS and 5 HS). MIG technique was used to deposit these patterns. The resulting samples were analysed from different perspectives; microstructures and mechanical properties were quantified and compared .

5.2 Conclusions

The most significant results of this study can be concluded as follows:

1. The WAAM samples built by different deposition patterns (longitudinal, transverse, right network, oblique and oblique network) showed a diversity of microstructure in different regions. Microscopy generally showed coarse equiaxed grains in the lower regions، fine equiaxed grains in the middle regions and columnar grains in the upper regions.

2. The effect of the forging process on samples built with the different deposition patterns was limited to the upper regions of the deposited material where the resulting microstructures were elongated grains.

3. The hardness of WAAM samples deposited with the different patterns without forging and with cold forging by (3 HS and 5 HS) significantly increased while moving from the upper to the lower regions, where the pearlite content was more as a result of the dilution.

4. The hardness of the samples forged by (5) HS was higher than that of those forged by (3) HS. The maximum hardness was (258 HV) for the sample built with the oblique network pattern and forged by (5) HS, while the minimum hardness was (170 HV) for the sample built longitudinally without forging.

5. Cold forging introduced, in general, a noticeable increase in tensile strength of the specimens extracted from the different samples. The highest average tensile strength value was (562 MPa) for the sample built longitudinally and forged by (3) HS. The fracture mode was significantly ductile.

6. The lowest average tensile strength value was (263MPa) for the sample built transversely, and the fracture mode was brittle.

5.3 Recommendations

The following is a summary of recommendations for further work:

1. The impact toughness test can be carried out for WAAM samples.

2. Other WAAM method can be used to deposit layers of built parts such as laser additive processing (LAM) or gas tungsten arc welding (GTAW).

3. It is possible to use hot forging after the deposition process.

References

1. Liberini M, Astarita A, Campatelli G et al (2017) Selection of optimal process parameters for wire arc additive manufacturing. Procedia CIRP 62:470–474.

2. Bekker ACM, Verlinden JC (2018) Life cycle assessment of wire +arc additive manufacturing compared to green sand casting and CNC milling in stainless steel DC Power Electrode wire Nozzle Shielding gas Arc Weld pool Workpiece Substrate. J Clean Prod 177:438–447.

3.Ford, S., & Mélanie, D. (2016), Additive Manfacturing and sustainability: an exploratory study of the advantages and challenges. Journal of Cleaner Production.

4. Ding D, Pan Z, Cuiuri D, Li H (2015), A multi-bead overlapping model for robotic wire and arc additive manufacturing (WAAM). Robot Comput IntegrManuf 31:101–110.

5. Shen C, Pan Z, Cuiuri D et al (2016) In-depth study of the mechanical properties for Fe3Al based iron aluminide fabricated using the wire-arc additive manufacturing process. Mater Sci Eng A 669:118–126.

6. FrazierWE (2014) Metal additive manufacturing: a review. JMater Eng Perform 23:1917–1928.

7. Das S, Bourell DL, Babu SS (2016) Metallic materials for 3D printing. MRS Bull 41:729–741

8. Williams SW, Martina F, Addison AC, Ding J, Pardal G, Colegrove P. Wire + arc additive manufacturing. Mater Sci Technol 2016;32:641–7.

9. Campbell RI, De Beer DJ, Pei E. Additive manufacturing in South Africa: Buildingon the foundations. *Rapid Prototyping Journal*. 2011 Mar 8;17:156–162.

10.Dizon,J.R.C.,EsperaJr,A.H.,Chen,Q.,&Advincula,R.C.(2018).Mechanicalcharacterizationof3D-printedpolymers.AdditiveManufacturing,20,44-67.

11.Core, B. 3D Printing 2019–2029 Technology and Market Analysis; IDTechEx:Cambridge,UK,2019.

12. د.عبد الواحد كاظم راجح(2016) ، الميتالورجيا الهندسية والمواد المتقدمة، جامعة بابل.

13. Purohit R. K. (2005), *Material Science and Processes*, Scientific Publishers Journals Dept., INDIA.

14. Hashmi M. S. J. (2017), *Comprehensive Materials Finishing: Finish*

Machining and Net-shape Forming, Vol 1, IRELAND.

15. Colas R. and Totten G. E. (2016), *Encyclopedia of Iron, Steel, and Their Alloys*, Vol 1, CRC press.

16. Totten G. E. (2006), *Steel heat treatment: metallurgy and technologies*, CRC press.

17. Steels L. A. (2001), High-Strength Low-Alloy Steels.

18. Tuttle R. (2018), *Alloy Steels*, 1st ed., Saginaw Valley State University,USA.

19. Avner S. H. (1974), Introduction to physical metallurgy, Vol. 2, pp.481-497, New York: McGraw-Hill.

20. Gibson I, Rosen DW, Stucker B. Additive Manufacturing Technologies. NewYork: Springer; 2014.

21. Huang SH, Liu P, Mokasdar A, Hou L. Additive manufacturing and itssocietalimpact: A literature review. The International Journal of Advanced Manufacturing Technology. 2013 Jul 1;67(5–8):1191–1203.

22. Wohlers, T. (2013, 02). *Industry Briefing*. Retrieved from Wohlers Associates.

23. ASTM F2732. (2013, 09 9). *www.astm.org.* Retrieved 01 30, 2017, from ASTM International.

24. Gibson, I., Rosen, D., &Stucker, B. (2015). *Additive Manufacturing Technologies.* New York: Springer.

25. Sames, W. J., List, F. A., Pannala, S., Dehoff, R. R., &Babu, S. S.(2016). *The metallurgy and processing science of metal additive manufacturing.* International Materials Reviews.

26.Sciaky. (2017). *Sciaky*. Retrieved 03 12, 2017, from Advantages of Wire AM vs. Powder AM.

27. Derekar, K. S. (2018). A review of wire arc additive manufacturing and advances in wire arc additive manufacturing of aluminium. Materials science and technology, 34(8), 895-916.

28. Rodrigues, T. A., Duarte, V., Miranda, R. M., Santos, T. G., & Oliveira, J. P. (2019). Current status and perspectives on wire and arc additive manufacturing (WAAM). Materials, 12(7), 1121.

29. Ding, D., Pan, Z., Cuiuri, D., & Li, H. (2015). Wire-feed additive manufacturing of metal components: technologies, developments and future interests. The International Journal of Advanced Manufacturing Technology, 81(1), 465-481.

30. Ding, J., Colegrove, P., Mehnen, J., Ganguly, S., Almeida, P. S., Wang, F., & Williams, S. (2011). Thermo-mechanical analysis of Wire and

Arc Additive Layer Manufacturing process on large multi-layer parts. Computational Materials Science, 50(12), 3315-3322.

31. Almeida, P. M., & Williams, S. (2010). Innovative process model of Ti-6Al-4V additive layer manufacturing using cold metal transfer (CMT). In 2010 International Solid Freeform Fabrication Symposium. University of Texas at Austin.

32. Wu, B., Pan, Z., Ding, D., Cuiuri, D., Li, H., Xu, J., & Norrish, J. (2018). A review of the wire arc additive manufacturing of metals: properties, defects and quality improvement. Journal of Manufacturing Processes, 35, 127-139.

33. Antonini, J.M. (2014). *Health Effects Associated with Welding*. Comprehensive Materials Processing Volume 8, Pages 49-70

34. http://www.halversoncts.com

35. A dor Welding Limited, "Modern Arc Welding Technology", Oxford &IBH Publishing Co. Pvt. Ltd (Book).

36. GHOSH, K.S. 2022, FOUNDATION OF WELDING TECHNOLOGY.

37. J. P. KAUSHISH (2010), MANUFACTURING PROCESSES.

38. D. KOSHAL (2014) Manufacturing Engineer's Reference Book.

39. د .عبد السميع جاسم عبد الزهرة) 2000 (السيطرة على عيوب و تشوهات لحام الصلب الكاربوني، رسالة ماجستير، كلية هندسة المواد جامعة بابل.

40. Narayana K. L., Rmana S. V. and Krishna P. V. (2010), *Production Technology*, 2nd ed., I.K. International Publishing House Pvt.Ltd.

41. Kiran D. V. and Joona S. (2014), *Experimental Studies on Submerged Arc Welding Process*, Journal of Welding and Joining (Vol. 32, No. 3).

42. Radhakrishnan V. M. (2008), *Welding Technology and Design*, New Age International Pvt. Ltd. Publishers.

43. Avner S. H. (1974), *Introduction to physical metallurgy*, Vol. 2, pp.481-497, New York: McGraw-Hill.

44. K Weman, G Lindén (2006), MIG welding guide

45. E. O. Ogundimu1, E. T. Akinlabi and M. F. Erinosho (2019), Comparative Study between TIG and MIG Welding Processes.

46. O.S. Ogbonna, S.A. Akinlabi, N. Madushele, P.M. Mashinini and A. A. Abioye(2019), Application of MIG and TIG Welding in Automobile Industry.

47. S.R. Patil, CA Waghmare (2013), Optimization of MIG welding parameters for improving strength of welded joints.

48. Khanna O. P. (1980), *Welding Technology: A textbook for Engineering Students*, Dhanpat Rai and Sons, 1st ed, Delhi.
49. American Welding Society (AWS) (2007), *Specification for Low-Alloy Steel Electrodes and Fluxes for Submerged Arc Welding*, 5th ed.
50. ESAB (2001), *Welding Handbook*, Consumable for manual and automatic welding, 6th ed.
51. KAUSHISH J. P. (2010), *MANUFACTURING PROCESSES,* 2nd ed., PHI Learning Private Limited, New Delhi.
52. Gandy D. (2007), *Carbon Steel Handbook*, EPRI Project Manager.

53. Mandal S. K. (2014), *Steel Metallurgy*, McGraw-Hill Education(India) Private Limited.
54. Talas S. (2010), *The assessment of carbon equivalent formulas in predicting the properties of steel weld metals,* Kocatepe University, Technical Education Faculty, Turkey. Elsevier Ltd.
55. Jeffus L. (2011), *Metal Fabrication Technology for Agriculture*, 2nd ed., Cengage Learning.
56. د.قحطان خلف الخزرجي و عبد الجواد محمد محمد احمد الشريف (1988) ، تكنلوجيا اللحام،جامعة بغداد.
57. Baily F. W. J (1972), *Fundamentals of engineering metallurgy and Materials*, 5th ed. London.

58. Lancaster J. F. (1980), *Metallurgy of Welding*, 3rd ed. (Allen and Unwin,
London UK).

59. Houldcroft P T and John R (2004), *Welding and Cutting: A Guide to Fusion*
Welding and Associated Cutting Processes, Woodhead Publishing Limited.

60. Jefferson, T. B., & Woods, G. (1966), *Metals and How to Weld Them*, James F. Lincoln Arc Welding Foundation 2nd ed., Cleveland.
61. Technical committee, Indian institute of Welding, Bangalore branch. (Dec., 1977) *Welding Metallurgy, technology and quality assurance*, Venue:Bangalore.
62. Amani J. (2011), *Effect of Submerged Arc Welding Parameters on the Microstructure of SA516 and A709 Steel Welds.*

63. د .عبد الرزاق اسماعيل خضر و د.نوفل محمد حسين (1993) ، تكنولوجيا اللحام، الجامعة التكنولوجية.

64. Kuppan T. (2000), *Heat Exchanger Design Handbook,* Marcel Dekker, Inc.

65. Wang, L., Suo, Y., Liang, Z., Wang, D., & Wang, Q. (2019).Effect of titanium powder on microstructure and mechanical properties of wire + arc additively manufactured Al-Mg alloy. Materials Letters, 241, 231-234.

66. Näsström, J., Brückner, F., & Kaplan, A. F. (2018). Measuring the effects of a laser beam on melt pool fluctuation in arc additive manufacturing .Rapid Prototyping Journal.

67. Duarte, V. R., Rodrigues, T. A., Schell, N., Miranda, R. M., Oliveira, J. P., &Santos, T. G. (2020). Hot forging wire and arc additive manufacturing (HF-WAAM).Additive Manufacturing,35, 101193.

68. Liu, J., Xu, Y., Ge, Y., Hou, Z., & Chen, S. (2020). Wire and arc additive manufacturing of metal components : a review of recent research developments.The International Journal of Advanced Manufacturing Technology ,111(1), 149-198.

69. Taylan Altan, Gracious Ngaile, Gangshu Shen- "Cold and Hot Forging-Fundamentals and Applications", Handbook by ASM International-February 2005

70. M.S.Sekhon,G.S.Barr and Sukhrajsingh.(2014),"A six sigma approach to detect forging defects in a small scale industry: A case study" ,International Journal of Engineering and Technical Research Publications,Vol.2No8, pp.33– 40.

71 Mathew, C.,Koshy, J.and Verma, D.(2013),"Study of Forging Defects in Integral Axle Arms", International Journal of Engineering and Innovative Technology, Vol.2No. 7, pp. 322-326.

72. AKTAKKA G.(2006), *Analysis of warm forging process.*

73. A. Bhaduri, "Forging," in Springer Series in Materials Science, 2018.
74. M. G. Rathi and N. A. Jakhade, "An Overview of Forging Processes with Their Defects," Int. J. Sci. Res. Publ., 2014
75. V. Bhoyar, S. Umredkar(2018) *Manufacturing Processes Part II: A Brief Review on Forging*. International Journal of Innovations in Engineering and Science, Vol 5, No.1

76.Campbell TA, Ivanova OS. 3D printing of multifunctional nanocomposites. Nano Today 2013;8:119-20.

77.Gu D, Meiners W, Wissenbach K, Poprawe R. Laser additive manufacturing of metallic components: materials, processes and mechanisms. International Materials Reviews 2012;57:133-64.

78.Mohr, S., Khan, O. (2015). '3D Printing and Supply Chains of the Future'. *Innovations and Strategies for Logistics and Supply Chains,* pp. 148 – 174.

79.Ford, S., Despeisse, M. (2016) 'Additive manufacturing and sustainability: an exploratory study of the advantages and challenges',

Journal of Cleaner Production, 137, pp. 1573-1587. doi:10.1016/j.jclepro.2016.04.150

80. T. Ron, G. K. Levy, O. Dolev, A. Leon , A. Shirizly and E. Aghion (2019). *Environmental Behavior of Low Carbon Steel Produced by a Wire Arc Additive Manufacturing Process*. University of the Negev, Beer-Sheva 8410501, Israel.

81. Ali W., Qin X., Xiong J., Wang H., Muhammad M., Arfan M.(2019) *Directional Tensile properties of steel structure manufactured by robotic assisted GMAW additive manufacturing*. Northwestern Polytechnical University Xi'an, China.

82. Mehran R. , Mahya G. , Alireza V. N. , Ali N.(2019). *Microstructural evolution and mechanical properties of a low-carbon low-alloy steel produced by wire arc additive manufacturing*. Faculty of Engineering and Applied Science, Memorial University of Newfoundland, St. John's, NL A1B 3X5, Canada.

83. Duarte, V. R., Rodrigues, T. A., Schell, N., Miranda, R. M., Oliveira, J. P., &Santos, T. G. (2020). *Hot forging wire and arc additive manufacturing (HF-WAAM).Additive Manufacturing*,*35*, 101193.

84. Van T. L., Henri P. (2020). *On the use of gas-metal-arc-welding additive manufacturing for repurposing of low-carbon steel components: microstructures and mechanical properties.* Institute of Research and Development, Duy Tan University, Da Nang 550000, Vietnam.

85. E. Aldalur, F. Veiga, A. Suarez, J. Bilbao, A. Lamikiz. (2020). *High deposition wire arc additive manufacturing of mild steel: Strategies and heat input effect on microstructure and mechanical properties.* Advanced Manufacturing Department, Paseo Mikeletegi 7, 20009 San Sebasti´an, Spain.

86. Tiago A. R., V. R. Duarte, D. Tomás, Julian A. Avila, J. D. Escobar, Emma Rossinyol, N. Schell, Telmo G. Santos, J. P. Oliveira.(2020). *In-situ strengthening of a high strength low alloy steel during Wire and Arc Additive Manufacturing (WAAM).* Department of Mechanical and Industrial Engineering, NOVA School of Science and Technology, Universidade NOVA de Lisboa, 2829-516 Caparica, Portugal.

87. Pattarawadee Poolperm, Wasawat Nakkiew and Nirut Naksuk. (2021). *Application of MIG Welding Process of Mild Steel Wire in Additive Manufacturing.* Key Engineering Materials ISSN: 1662-9795, Vol. 877, pp 73-79

88.http://bbnsteelplate.com/news/astm-a36-steel-equivalent-indian-standardis-is2062_928.

89. AISI 5155: Low Chromium Alloy Steel(1979) Producer or Source: Alloy steel mills and foundries, Volume 28, Issue 11.

90. ASM, Metals Handbook (1975) "Welding and Brazing" 8th ed.

91. El-Rayes M. M., El-Danaf E. A.(2012), *The influence of multi-pass friction stir processing on the microstructural and mechanical properties of Aluminum Alloy 6082*. Volume: 212, Issue: 5, Pages: 1157 - 1168

92. B. Bagheri, M. Abbasi, A. Abdollahzadeh (2020), *Effect of second-phase particle size and presence of vibration on AZ91/SiC surface composite layer produced by FSP*.

93. L.Ceschini, G. Minak, A. Morri (2009), *Forging of the AA2618/20 vol.% Al2O3p composite: Effects on microstructure and tensile properties*.

94. X. Jin, S. Chen, L. Rong(2018), *Microstructure modification and mechanical property improvement of reduced activation ferritic/martensitic steel by severe plastic deformation*.

الخلاصة

في الآونة الأخيرة، تعد عملية ترسيب اللحام القائمة على الغاز الخامل (MIG) واحدة من عمليات التصنيع المضافة القائمة على الترسيب (AM). لقد خلقت هذه التقنية اهتمامًا كبيرًا نظرًا للمزايا التي تقدمها كونها قادرة على إنتاج أجسام معدنية ثقيلة ومعقدة تعمل بكامل طاقتها. نظرًا لمعدلات الترسيب العالية، وكفاءة المواد والطاقة العالية، وانخفاض تكاليف الاستثمار، ومتطلبات الإعداد وبيئة العمل الأكثر بساطة، فقد أصبحت طريقة AM المعدنية قابلة للتطبيق. في الوقت الحاضر، تُستخدم تقنيات AM في نطاق واسع من التطبيقات مثل صناعة السيارات وصناعة الأدوات الآلية وشركات الطيران ... إلخ.

تهدف الدراسة بشكل أساسي التحقق من تأثير مجموعة متنوعة من أنماط الترسيب وعملية الطرق على البارد بضربات طرق مختلفة (3 HS) و (5 HS)على البنية المجهرية والخصائص الميكانيكية للمواد الفولاذية المبنية على ركيزة من فولاذ واطئ السبائك بواسطة عملية MIG. أجريت التجارب باستخدام لحام MIG نصف آلي على ركيزة من الفولاذ الواطئ السبائك (AISI 5155) باستخدام سلك فولاذي مطلي بالنحاس (ER70S.6) لبناء العينات المصنعة باستخدام خمسة أنماط ترسيب مختلفة (طولية، عرضية ، شبكة ، مائلة وشبكة مائلة). تم إجراء العديد من الفحوصات لتقييم العينات المبنية مع وبدون عملية الطرق باستخدام المجهر الضوئي، والماسح المجهري الإلكتروني باستخدام مطياف تشتت الطاقة وتصوير الكسر، بالإضافة إلى الاختبارات الميكانيكية مثل الصلادة الدقيقة ومقاومة الشد.

أظهرت النتائج أن العينات المبنية بواسطة أنماط الترسيب المختلفة أظهرت تنوعًا في البنية المجهرية في مناطق مختلفة. أظهر الفحص المجهري بشكل عام الحبيبات الخشنة المتساوية المحاور في المناطق السفلية، والحبيبات الدقيقة المتساوية المحاور في المناطق الوسطى والحبيبات الطولية في المناطق العليا. اقتصر تأثير عملية الطرق على العينات المبنية بأنماط الترسيب المختلفة على المناطق العليا من المادة المترسبة حيث كانت البنى المجهرية الناتجة عبارة عن حبيبات مستطالة. كان تأثير (5 HS) أعلى من تلك التي تم طرقها بواسطة (3 HS) كانت أقصى صلادة (258 HV) للعينة المبنية على نمط الشبكة المائلة والمطروقة بواسطة(5 HS) بينما الصلادة الدنيا كانت (170 HV) للعينة المبنية طولياً بدون طرق. قدم الطرق على البارد بشكل عام زيادة ملحوظة في مقاومة الشد للعينات المستخرجة من العينات المختلفة وكانت أعلى قيمة لمتوسط مقاومة الشد (562 MPa) للعينة المبنية طولياً والمطروقة بمقدار (3 HS) .كان وضع الكسر مطيلي بشكل ملحوظ، أما أقل قيمة لمتوسط مقاومة الشد فكانت (263 MPa) للعينة المبنية عرضيا، وكان وضع الكسر هشاً.

وزارة التعليم العالي والبحث العلمي

جـــــــــــامعة بـــابـــــــل

كـــــليـــــــة هندسة المـــــــواد

قســـــــــم هندسة المعـــــادن

تحسين البنية المجهرية والخواص الميكانيكية للفولاذ المطاوع المصنع بالإضافة بواسطة القوس الكهربائي المعدني الغازي باستخدام عملية الطرق

رسالة

مقدمة الى قسم هندسة المعادن في كلية هندسة المواد/جامعة بابل وهي جزء من متطلبات نيل درجة الماجستيرفي هندسة المواد/المعادن

من قبل

أرزاق سليم عبد علي

بكالوريوس هندسة المواد(2018)

بإشراف

ا.د. سعد حميد الشافعي

ا.م.د. عبد السميع جاسم عبد الزهرة الكلابي

1445هـ **2023 م**